A computational framework for modeling cell-matrix interactions in soft biological tissues

**Jonas F. Eichinger · Maximilian J. Grill · Iman Davoodi Kermani ·
Roland C. Aydin · Wolfgang A. Wall · Jay D. Humphrey · Christian J.
Cyron**

Abstract Living soft tissues appear to promote the development and maintenance of a preferred mechanical state within a defined tolerance around a so-called set-point. This phenomenon is often referred to as mechanical homeostasis. In contradiction to the prominent role of mechanical homeostasis in various (patho)physiological processes, its underlying micromechanical mechanisms acting on the level of individual cells and fibers remain poorly understood, especially, how these mechanisms on the microscale lead to what we macroscopically call mechanical homeostasis. Here, we present a novel finite element based computational framework that is constructed bottom up, that is, it models key mechanobiological mechanisms such as actin cytoskeleton contraction and molecular clutch behavior of individual cells interacting with a reconstructed three-dimensional extracellular fiber matrix. The framework reproduces many experimental observations regarding mechanical homeostasis on short time scales (hours), in which the deposition and degradation of extracellular matrix can largely be neglected. This model can serve as a systematic tool for future *in silico* studies of the origin of the numerous still unexplained experimental observations about mechanical homeostasis.

Keywords mechanical homeostasis · growth and remodeling · cell-extracellular matrix interaction · discrete fiber model · finite element method

Declarations

Conflicts of interest/Competing interests
Not applicable

Availability of data and material
Not applicable

Code availability
Not applicable

J. F. Eichinger · M. J. Grill · I. Davoodi Kermani · W. A. Wall
Institute for Computational Mechanics, Technical University of Munich,
Garching, 85748 Germany

J. F. Eichinger · C. J. Cyron
Institute of Continuum and Materials Mechanics, Hamburg University of Technology,
Hamburg, 21073 Germany

J. D. Humphrey
Department of Biomedical Engineering, Yale University,
New Haven, CT 06520 USA

R. C. Aydin · C. J. Cyron
Institute of Material Systems Modeling, Helmholtz-Zentrum Geesthacht,
Geesthacht, 21502 Germany
E-mail: christian.cyron@tuhh.edu

1 Introduction

Living soft tissues, in contrast to classical engineering materials, usually seek to establish and maintain a mechanical state that is not stress-free. This behavior of living soft tissues is often referred to as *mechanical homeostasis*, and it plays a key role in the control of form and function in health and disease (Lu et al., 2011; Humphrey et al., 2014; Ross et al., 2013; Cox and Erler, 2011; Bonnans et al., 2014). Intra-cellular structures such as the actomyosin cytoskeleton are physically coupled to the surrounding extracellular matrix (ECM) via transmembrane protein complexes such as integrins that can cluster to form focal adhesions (Cavalcanti-Adam et al., 2007; Lerche et al., 2019). This coupling allows cells to receive mechanical cues from their environment, transduce these cues into intra-cellular signals, and react, for example, by adapting cellular stress and thereby also the stress of the surrounding ECM. Physical interactions between cells and ECM have been shown to control various processes on the cellular scale such as cell migration (Kim et al., 2020; Xie et al., 2017; Hall et al., 2016; Grinnell and Petroll, 2010), differentiation (Chiquet et al., 2009; Mammoto et al., 2012; Zemel, 2015; Seo et al., 2020) and survival (Bates et al., 1995; Zhu et al., 2001; Sukharev and Sachs, 2012; Schwartz, 1995), and are therefore fundamental for health and in disease of entire tissues and organs.

To study the micromechanical foundations of mechanical homeostasis experimentally, tissue culture studies with cell-seeded collagen or fibrin gels have attracted increasing interest over the past decades (Eichinger et al., 2021). Circular free-floating gels, when seeded with fibroblasts, exhibit a strong compaction over multiple days in culture due to cellular contractile forces (Simon et al., 2014, 2012). Studies of such gels whose compaction is prevented by boundary constraints typically show a two-phase response. First, tension in the gels rapidly increases to a specific value, the so-called homeostatic tension (phase I), and then remains largely constant (phase II) for the rest of the experiment (Marenzana et al., 2006; Brown et al., 1998; Ezra et al., 2010; Eichinger et al., 2020; Brown et al., 2002; Courderot-Masuyer, 2017; Campbell et al., 2003; Dahlmann-Noor et al., 2007; Karamichos et al., 2007; Sethi et al., 2002). If the gel is perturbed in phase II, for example, by an externally imposed deformation, cells appear to promote a restoration of the homeostatic state (Brown et al., 1998; Ezra et al., 2010). Despite substantial research efforts over decades, the exact interplay between cells and surrounding tissue that is crucial for mechanical homeostasis and other related phenomena such as duro-

taxis still remains poorly understood to date (Eichinger et al., 2021).

Computational studies in this field have focused primarily on decellularized ECM systems to study the micromechancial and physical properties of networks of fibers (Heussinger and Frey, 2007; Mickel et al., 2008; Lindström et al., 2010; Chatterjee, 2010; Broedersz et al., 2011; Stein et al., 2010; Ronceray et al., 2016; Cyron and Wall, 2012; Cyron et al., 2013b,a; Lang et al., 2013; Motte and Kaufman, 2013; Müller et al., 2014; Jones et al., 2014; Lee et al., 2014; Müller et al., 2015; Mauri et al., 2016; Dong et al., 2017; Humphries et al., 2018; Zhou et al., 2018; Bircher et al., 2019; Domaschke et al., 2019, 2020). Current computational models of cell-ECM interactions often suffer from shortcomings – most are limited to two dimensions and just one or two cells (Wang et al., 2014; Abhilash et al., 2014; Notbohm et al., 2015; Jones et al., 2015; Kim et al., 2017; Grimmer and Notbohm, 2017; Burkel et al., 2018; Humphries et al., 2017). The importance of the third dimension for the physics of fiber networks is well-known (Baker and Chen, 2012; Jansen et al., 2015; Duval et al., 2017), and it can be assumed that collective interactions between more than just two cells play important roles in mechanical homeostasis. Moreover, current models typically rely in many crucial aspects on heuristic assumptions (Nan et al., 2018; Zheng et al., 2019) and almost all of them assume simple random fiber networks (e.g., based on Voronoi tesselations) that do not match the specific microstructural characteristics of actual collagen gels or tissues. What remains wanting is a robust, computationally efficient three-dimensional model of cell-fiber interactions, where the microstructure of the fiber network realistically resembles real collagen gels and tissues and which is efficient enough to enable simulations with several cells. Such a computational model can be expected to help unravel the micromechanical and molecular foundations of mechanical homeostasis.

In this paper, we introduce such a computational model. It is based on the finite element method and relies on a strong experimental foundation. It can be used to test various hypotheses with regard to the micromechanical principals of mechanical homeostasis. It can also help to identify promising future experiments. The model focuses on mechanical aspects of homeostasis by concentrating on the physical interactions of cells with surrounding matrix fibers and thus neglects direct modeling of biochemical phenomena. The paper focuses on a detailed description of the computational framework, but examples are used to demonstrate the physical validity of this framework and to illustrate the opportunities it will open up. It will be seen that this frame-

work captures well key observations from experiments on short time scales (in which deposition and degradation of tissue fibers can be neglected) thus helping to explain the underlying physics.

2 Models and methods

To study the physical foundations of mechanical homeostasis in soft biological tissues on short time scales (hours), our framework models i) interlinked ECM-like fiber networks whose microstructure closely resembles that of actual collagen gels, ii) transmembrane proteins such as integrins which connect extra- to intra-cellular structures, and iii) the contractile activity of the cytoskeleton. In the following we describe the mathematical and computational details of our model.

2.1 Construction of representative volume elements (RVE)

Computational modeling of soft tissues on the level of discrete fibers and individual cells remains intractable for large tissue volumes, noting that 1 ml of ECM may contain over one million cells. Therefore, we use RVEs as structurally typical samples of the considered tissue (Fig. 1 A). Building on our previous work on biopolymer networks (Cyron and Wall, 2012; Cyron et al., 2013b,a; Grill et al., 2020), we constructed physically realistic three-dimensional fiber networks from confocal microscope images of actual collagen gels (Fig. 1 A). Following Lindström et al. (2010) and Davoodi-Kermani et al. (2021), we assumed that the mechanical properties of collagen fiber networks are predominantly governed by three descriptors, namely, the valency (number of fibers connected to a network node), the free-fiber lengths between adjacent nodes (herein also referred to as fiber length), and the angles between the fibers joining at the nodes (which can be quantified by the cosine of the angles between any pair of fibers joining at a node). These descriptors vary in the network across the fibers and nodes by following certain statistical distributions. Using the computational procedure described in Appendix A1, which is motivated by Lindström et al. (2010); Yeong and Torquato (1998) and briefly illustrated in Fig. 1, we ensured that the statistical distributions of valency, free-fiber length and inter-fiber cosines closely matched those of actual collagen fiber networks. The computational procedure to produce such networks has been implemented in a short C++ program which is available under the BSD 3-Clause License as the repository `bionetgen` hosted at `https://github.com/bionetgen/bionetgen`.

2.2 Mechanical network model

We used the finite element method to model the mechanics of our fibrous RVE. Individual fibers were modeled as geometrically exact beam finite elements based on the non-linear Simo-Reissner theory (Reissner, 1981; Simo, 1985; Simo and Vu-Quoc, 1986) and a hyperelastic material law. This beam theory captures the modes of axial tension, torsion, bending and shear deformation and is appropriate for large deformations. Thus, our finite element model of the fiber network can capture all essential modes of mechanical deformation. If not stated otherwise, covalent bonds between fibers were modeled as rigid joints coupling both translations and rotations. We chose the dimensional and constitutive parameters to mimic collagen type I fibers as the most abundant structural protein of the ECM. Fibers are assumed to have circular cross-sections with a diameter of $D_f = 180 \ nm$ (Van Der Rijt et al., 2006) and elastic moduli of $E_f = 1.1 \ MPa$ (Jansen et al., 2018). Assuming curvilinear fibers with circular cross-section of diameter D_f, the average mass density of collagen ρ_c in the network RVE was calculated as

$$\rho_c = \frac{L_{tot} D_f{}^2 \pi}{V_{4\text{RVE}} v_c} \tag{1}$$

according to Stein et al. (2008), where L_{tot} is the sum of all individual fiber lengths, V_{RVE} the volume of the RVE, and $v_c = 0.73$ ml/g the specific volume of collagen fibers (Hulmes, 1979).

2.3 Fiber-to-fiber cross-linking

A native ECM consists of myriad structural constituents, including collagen and elastin, which usually form networks to provide mechanical support to the resident cells. To form these networks, covalent cross-links are formed via the action of enzymes such as lysol oxidase and transglutaminase, which can be produced by the cells (Simon et al., 2014). In addition to covalent bonds, transient hydrogen bonds or van-der-Waals bonds contribute further to the mechanical integrity of the ECM (Kim et al., 2017; Ban et al., 2018).

To model initially existing covalent bonds between fibers, we permanently connect individual fibers joining at nodes of our initially generated network by rigid joints. To model the formation of additional transient and covalent bonds, we define so called binding spots on all fibers (Fig. 2). If during the simulation it happens
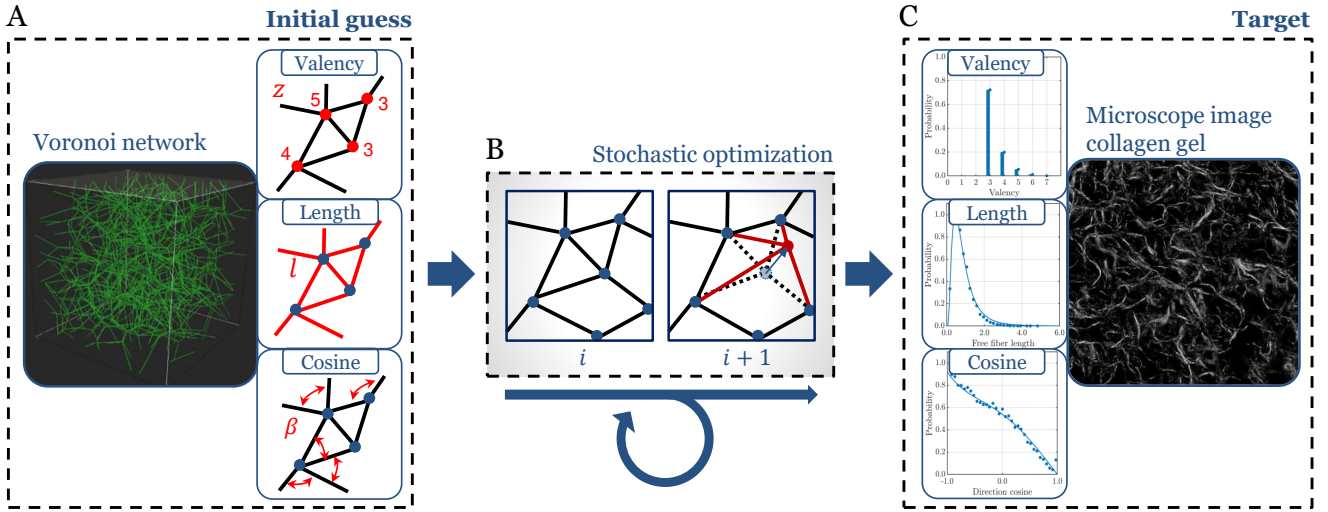
Fig. 1 Schematic of the network construction process. (A) Random fiber network geometries based on Voronoi tesselation are used as the initial configuration. Valency, length and cosine distribution are used as descriptors of the network geometry for which target distributions are given. (B) By iterative random displacements of arbitrary nodes in the network and accepting these displacements based on their impact on the system energy, which penalizes deviations of the geometric descriptors from their target distributions, one arrives after a number of stochastic steps at a configuration with the desired distribution of the geometric descriptors of interest. (C) Microscope images of collagen gels are used to determine the target distributions for the descriptors of the network.

that the distance between two binding spots on distinct filaments falls within a certain critical interval, a new bond between the two filaments is established according to a Poisson process with an on-rate k_{on}^{f-f}. That is, within a subsequent time step Δt, a bond is assumed to form with a probability

$$p_{on}^{f-f} = 1 - \exp\left(-k_{on}^{f-f} \Delta t\right). \tag{2}$$

Newly established bonds are modeled by initially stress-free beam elements. Bonds established this way during the simulation can also dissolve. This process is again modeled by a Poisson process with an off-rate k_{off}^{f-f}, yielding in each time step Δt an unbinding probability

$$p_{off}^{f-f}(F) = 1 - \exp\left(-k_{off}^{f-f}(F) \cdot \Delta t\right). \tag{3}$$

The off-rate is in general affected by the force F acting on the bond because transient chemical bonds under mechanical loading are typically less (though in certain regimes more) stable than load-free bonds (Bell, 1980). This phenomenon can be modeled by a force-dependent off-rate

$$k_{off}^{f-f}(F) = k_{off,0}^{f-f} \ \exp\left(\frac{F\Delta x}{k_B T}\right), \tag{4}$$

with Δx a characteristic distance, k_B the Boltzmann constant, and T the absolute temperature (Bell, 1980). $\Delta x > 0$ was chosen so that the bond weakens under tension, a bond behavior that is often referred to as

slip-bond behavior. By choosing $k_{off,0}^{f-f} = 0$, we can resemble new covalent bonds formed during our simulations, whereas $k_{off,0}^{f-f} > 0$ mimics transient bonds.

2.4 Cell-ECM interaction

Cells in soft tissues can mechanically connect to surrounding fibers by integrins and exert stress on them by focal adhesions. A focal adhesion usually includes an actin stress fiber bundle in the cytoskeleton that connects the nucleus of the cell with the integrins of a cluster and can actively contract. Based on experimental observations, we restricted the maximal number of focal adhesions per cell to $N_{FA,max} = 65$ (Horzum et al., 2014; Kim and Wirtz, 2013; Mason et al., 2019) (Fig. 3 B on the left shows 3 focal adhesions). It has been shown experimentally that roughly $N_{i,FA,max} = 1000$ integrins are involved in one focal adhesion (Wiseman, 2004; Elosegui-Artola et al., 2014). These integrins are organized in so-called integrin clusters of roughly $20-50$ integrins (Changede et al., 2015; Cheng et al., 2020) (Fig. 3 C). We thus assume for each focal adhesion 50 integrin clusters containing a maximum of $N_{i,ic,max} = 20$ integrins each.

To model cell-mediated active mechanical processes in soft tissues, we model the cell centers as point-like particles. When these particles approach predefined integrin binding spots (with a distance of $d^{i-f} = 50nm$ to each other (López-García et al., 2010)) on the fibers within $\pm \Delta R$ around the cell radius R, a physical con-
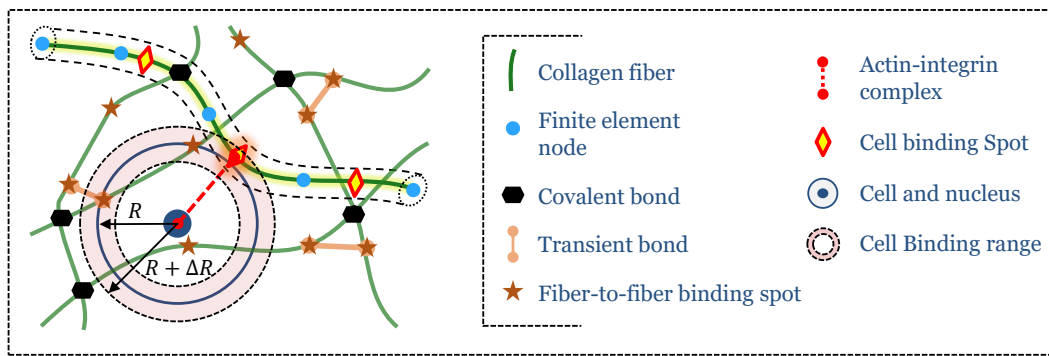
Fig. 2 Fiber network model: collagen fibers are modeled as beam-like mechanical continua discretized by beam finite elements. Nearby collagen fibers are connected by permanent (covalent) chemical bonds modeled as rigid joints. During the simulation additional transient bonds may stochastically form and dissolve between nearby binding spots of the fibers. These bonds are also modeled by short beam-elements transmitting forces and moments. Cells of radius R can attach to nearby collagen fibers if certain predefined cell binding spots on the surrounding fibers are within $R - \Delta R$ and $R + \Delta R$ around the cell.

nection between cells and fibers is assumed to form by a Poisson process similar to the one in Eq. (2), but with a specific on-rate k_{on}^{c-f} (see also Fig. 3 A). The actin stress fibers connecting the cell nucleus with the fibers surrounding the cells are modeled as elastic springs (Fig. 3 B and C) whose stress-free length evolves at some predefined rate $\dot{c}$ that can be calculated to match experimental data of different cell types. These stress fiber contract at a rate of $\dot{c} = 0.1 \frac{\mu m}{s}$ (Choquet et al., 1997; Moore et al., 2010). The force acting on a single integrin F_i can be computed according to

$$F_i = \frac{F_{SF}}{N_{i,bonded}}, \tag{5}$$

with F_{SF} being the force acting in the respective stress fiber and $N_{i,bonded}$ the number of currently bound integrins in the integrin cluster associated with the respective stress fiber.

In contrast to many previous approaches in which displacements have been prescribed in the neighborhood of cells to model their contraction, we are able to model a true two-way feedback loop between cell and ECM. Integrins have been shown experimentally to exhibit a so-called catch-slip bond behavior (Kong et al., 2009) whose unbinding can be modeled by a Poisson process with a force-dependent off-rate

$$k_{off}^{c-f}(F) = a_1 \exp\left(-\left(\frac{F - b_1}{c_1}\right)^2\right) \\ + a_2 \exp\left(-\left(\frac{F - b_2}{c_2}\right)^2\right) \tag{6}$$

whose parameters were determined via fits to the experimental data (Kong et al., 2009; Weng et al., 2016) (Fig. 3 D) and can be found in Table A2. While the average lifetime of most chemical bonds decreases monotonically with increasing force transmitted by the bond,

catch-slip bonds exhibit a regime where the bond stabilizes as the force increases. As illustrated in Fig. 3 D, this makes integrin bonds particularly stable for values of F_i in a range around $30 pN$. Recall that we model an integrin cluster as a system of 20 parallel integrins whose bonds form and dissolve according to the above specified on- and off-rates (Fig. 3 C). If at a certain point all bonds happen to have broken at the same time, the related integrin cluster is assumed to dissolve. It may, however, reform on the basis of a new (not yet contracted) stress fiber shortly thereafter with a binding rate k_{on}^{c-f}. If all clusters of a certain focal adhesion happen to dissolve at the same time, the focal adhesion as a whole is dissolved.

This model implies that many binding and unbinding events of integrins occur during the lifetime of a focal adhesion. This way, our model captures the chemical dynamics of the connection between cells and ECM fibers on different scales ranging from individual integrins to whole focal adhesions (Stehbens and Wittmann, 2014). Thereby, our model bots captures typical lifetimes of focal adhesions on the order of minutes and turnover rates of most proteins involved in the adhesion complex on the order of seconds.

2.5 Boundary conditions

As mentioned before, simulations of complete tissues on the cm-scale are computationally expensive with discrete fiber models; hence we have to study RVEs. A major challenge in the context of discrete fiber simulations is the imposition of deformations on the RVE to study its response to certain strains. To this end, most previous work of other groups requires that the nodes of the finite elements used to discretize fibers are located exactly on the boundary surfaces of the RVE
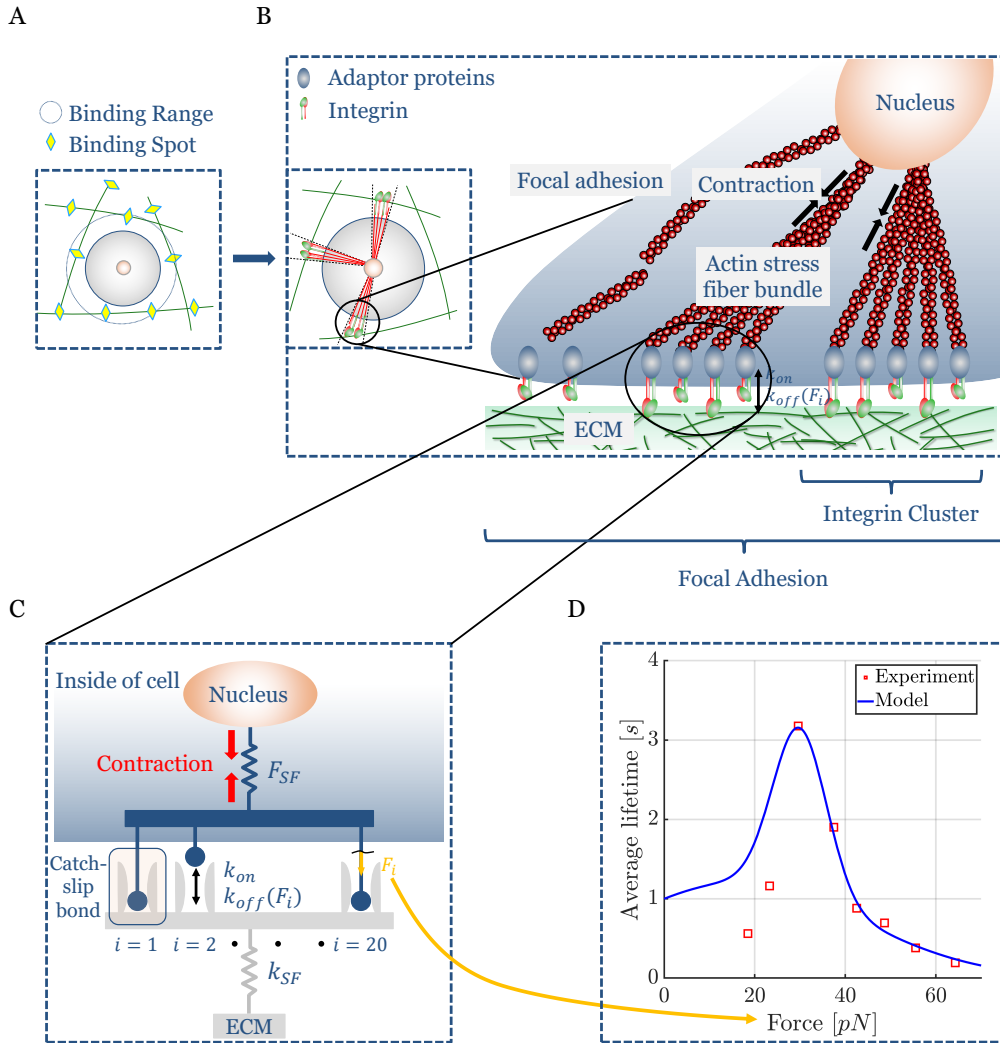
Fig. 3 (A) If cells lie within a certain distance from integrin binding spots on fibers, a focal adhesion can from with a certain probability. (B) A focal adhesion consists of around 1000 integrins connecting the intra-cellular actin cytoskeleton to the ECM fibers. Actin stress fibers connect the cell nucleus to the focal adhesions and are modeled as elastic springs that contract over time. (C) Each focal adhesion consists of numerous so-called integrin clusters, each formed by $20 - 50$ integrins. We assume that each integrin cluster is connected to one actin stress fiber. Integrins are modeled as molecular clutches, i.e., they bind and unbind according to specific binding kinetics. (D) Experiments have determined a catch-slip bond behavior for single integrins where the life time does not monotonically decrease with the mechanical force transmitted through the bonds but where there exists a regime where increasing forces increase the average life time of the bond. To avoid infinite off-rates in case of low forces, we chose a slightly higher life time for low forces compared to the experimental data of Kong et al. (2009).

where displacements are prescribed (Stein et al., 2010; Humphries et al., 2018; Abhilash et al., 2014; Burkel et al., 2018; Ban et al., 2018; Liang et al., 2016; Ban et al., 2019). Other approaches prescribe the displacements of nodes close to these surfaces (Lee et al., 2014). These methods share the problem that they do not ensure full periodicity across the boundaries where displacements are prescribed. To overcome this limitation, we developed a novel form of fully periodic boundary conditions for fiber networks that allows the imposition of complex multiaxial loading states. This approach ensures full periodicity across all surfaces of the RVE and

thereby minimizes computational artifacts due to finite-volume effects. The computational details of our algorithm are summarized in Appendix A2.

2.6 Search algorithm and parallel computing

To yield meaningful computational results, our RVEs have to be much larger than the characteristic microstructural features such as the free-fiber length between adjacent nodes. Using values for the cell density and collagen concentration in a physiologically reasonable range typically leads to a system size of the RVE that can be

solved only by parallel computing, including an efficient parallel search algorithm for the evaluation of all interactions between cells and fibers. We implemented such a search algorithm based on a geometrical decomposition of the computational domain in uniform cubic subdomains. The computational details of our parallelization are summarized in Appendix A3. Importantly, our approach does not require any fully redundant information on all processes, which enables a highly efficient parallelization on even a very large number of processors.

3 Results and discussion

The presented computational framework was implemented in our in-house research finite element code BACI (BACI, 2021). To ensure robustness, scalability and especially validity, we performed various computational simulations and compared the results with available experimental data. The default parameters used in our simulations can be found in Table A2.

3.1 Network construction

We first validated the network generation method described in Section 2. To this end, we created networks with different collagen concentrations and target descriptor distributions as observed by confocal microscopy in tissue culture experiments with collagen type I gels (Lindström et al., 2010; Nan et al., 2018). As shown in Fig. 4, our stochastic optimization method successfully generates networks with the desired distributions of valency, free-fiber length and direction cosine. Fig. 5 A demonstrates that our simulated annealing converged well toward the desired solution with an increasing number of random iteration steps.

### 3.2 Passive mechanical properties: stiffness

Next, we verified that our constructed, still acellular, networks have similar mechanical properties as actual collagen networks. To this end, we simulated simple uniaxial tensile tests with different collagen concentrations and compared the resulting values for the stiffness with values that have been collected in uniaxial experiments with collagen type I gels (Joshi et al., 2018; Alcaraz et al., 2011; Miroshnikova et al., 2011). We stretched a cubic simulation box with edge length $L = 245\mu m$ in one direction by applying displacement boundary conditions as described in Appendix A2 at a slow loading rate of $0.01\mu m/s$ up to a strain of 1.0%; strains around 1% have been shown to be the relevant

range when studying active, cell-mediated force development (Eichinger et al., 2020). Fig. 5 C demonstrates that the Young's moduli of the constructed networks match well with the values observed in tissue culture experiments. In our artificial RVE we found a power law dependence between the Young's modulus and the collagen concentration with an exponent of 1.33, very similar to the exponent of 1.22 found experimentally (Joshi et al., 2018).

3.3 Active mechanical properties: homeostatic tension

In this section we consider cell-seeded fiber networks to study the *active* mechanics of soft tissues. The tension that develops in constrained gels stems from the contractile forces exerted by the cells on the surrounding fibers. In initially stress-free collagen gels seeded with fibroblasts, the tension builds up over a couple of hours until it has reached a plateau value, the so-called homeostatic value (Marenzana et al., 2006; Brown et al., 1998; Ezra et al., 2010; Eichinger et al., 2020; Brown et al., 2002; Courderot-Masuyer, 2017; Campbell et al., 2003; Dahlmann-Noor et al., 2007; Karamichos et al., 2007; Sethi et al., 2002). Tissue culture experiments (Eichinger et al., 2020; Delvoye et al., 1991) have shown that the homeostatic tension depends on both cell and collagen concentration in the gel. We used this observation to validate our computational model. We created RVEs with an edge length of $L = 245\mu m$ and three different cell densities and collagen concentrations as studied experimentally in Eichinger et al. (2020). To increase the complexity of the RVE only gradually by adding cells, we still solely considered covalent bonds between matrix fibers. We then compared the cell-mediated active tension over time of our simulations to the one observed experimentally.

It is important to note that a direct (quantitative) comparison between experimental data and simulation results is difficult due to differing boundary conditions. Tissue culture experiments have at least one (traction-) free boundary (uniaxial gels have two, circular discs three), while we performed our simulations with RVEs with periodic boundary conditions applied in all directions (note also that a free boundary in a microscopic RVE would not resemble a free boundary of a macroscopic specimen). It has been shown, however, that the number of fixed boundaries has a crucial impact on the homeostatic plateau value (Eichinger et al., 2020). In the following, we compare the first Piola-Kirchhoff stresses, as the thickness of the gel samples over time is unknown. We assumed $A_{initial} = 1.6mm$ (knowing

A

B

C
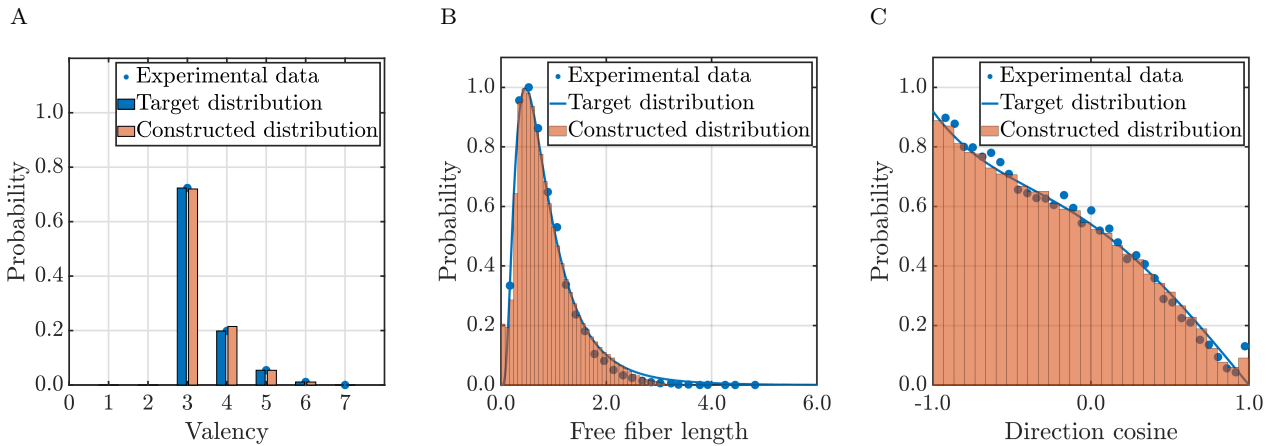
Fig. 4 Results of the network construction process for a collagen concentration of $2.5mg/ml$. (A) valency distribution, (B) free-fiber length distribution and (C) cosine distribution fit well the target distributions defined on the basis of experimental data taken from Nan et al. (2018) in (A) and from Lindström et al. (2010) in (B) and (C).

A

B

C
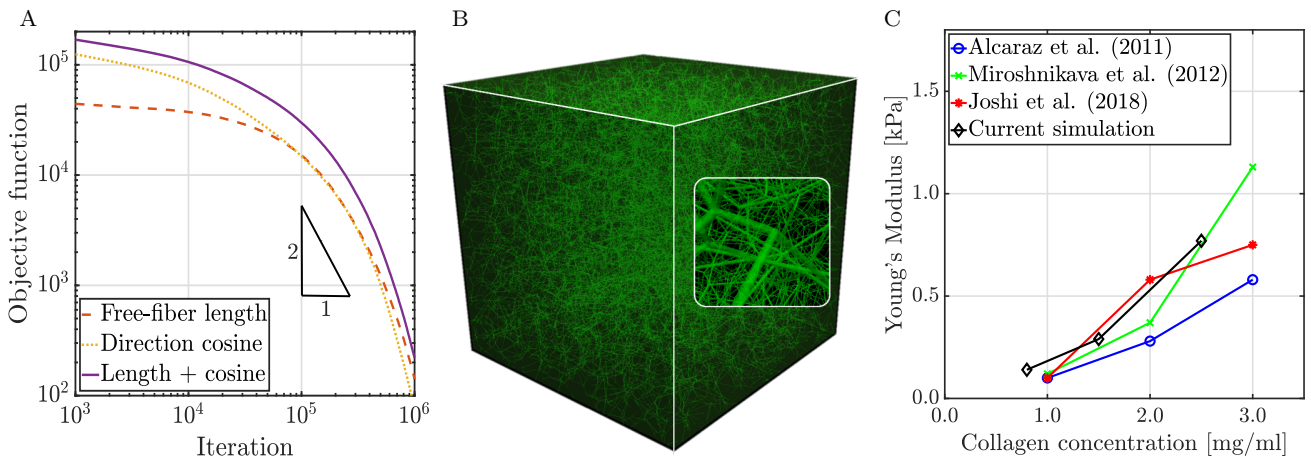
Fig. 5 (A) In the stochastic network construction with a collagen concentration of 0.8mg/ml in a cube of edge length $245\mu m$, the energy-type objective function according to Eq. (A5) is reduced during simulated annealing (in the studied range even superquadratically) by multiple orders of magnitude; (B) this optimization process yields RVE with a desired microstructure; (C) the effective Young's modulus at strains $< 1\%$ of RVE constructed this way match well with the ones observed in experiments (Joshi et al., 2018; Alcaraz et al., 2011; Miroshnikova et al., 2011).

it to be between $1.5mm$ and $2mm$) to fit best to our simulation data.

3.3.1 Variation of cell density

In this section we consider gels with a constant collagen density of $1.5mg/ml$. Cell densities of $0.2 \cdot 10^6$ cells/ml, $0.5 \cdot 10^6$ cells/ml and $1.0 \cdot 10^6$ cells/ml studied in Eichinger et al. (2020) translate in our simulations into 3, 8 and 15 cells per RVE, respectively. Fig. 6 A shows the evolution of the first Piola-Kirchhoff stress (true force/original area) generated in uniaxially constrained, dog-bone shaped collagen gels as observed experimentally. The gradient during the first $10h$ of the experiment and the homeostatic plateau level of stress increase with the cell density. Both features are observed also in our simulations and fit quantitatively well (Fig. 6 B and C). We

can therefore conclude that actin cytoskeleton contraction along with the focal adhesion dynamics described in Section 2.4 are sufficient mechanisms to reproduce this non-trivial relationship.

A crucial difference between experiments and simulations is the time scale. Whereas mechanical homeostasis develops over a couple of hours in the experiments, it does so within a couple of minutes in the simulation. Interestingly, this time scale of our simulations agrees well with that for which single cells in experiments on purely elastic substrates reach a homeostatic state (Weng et al., 2016; Hippler et al., 2020). Thus, a possible explanation for the difference between our simulations and the experimental data from Eichinger et al. (2020) may be that in tissues with numerous cells, complex interactions between the cells substantially delay the homeostatic state. Such interactions remain poorly

understood and are not yet accounted for in our computational framework. Another possible explanation for the different time scales in Fig. 6 A and B may be viscoelasticity due to collagen fibers moving within culture media, which is not included in our model in detail, and due to an increasing stiffness of the gel due to progressed polymerization when being placed in an incubator of 37°C for longer times. Finally, subtle aspects on the sub-cellular scale that are not included in our model may affect the time to reach the homeostatic state substantially because it is well-known that this time differs considerably for different cell types (Eichinger et al., 2021).

Fig. 7 A shows that the deformation of the matrix fibers around the cells in our simulations are on the order of $10\mu m$, which agrees well with experiments (Notbohm et al., 2015; Malandrino et al., 2019). Our simulation framework also reproduces the ability of cells to communicate via long-range mechanical interactions over several cell diameters (Fig. 7 B), which has also been observed experimentally (Kim et al., 2017; Ma et al., 2013; Shi et al., 2013; Baker et al., 2015; Mann et al., 2019).

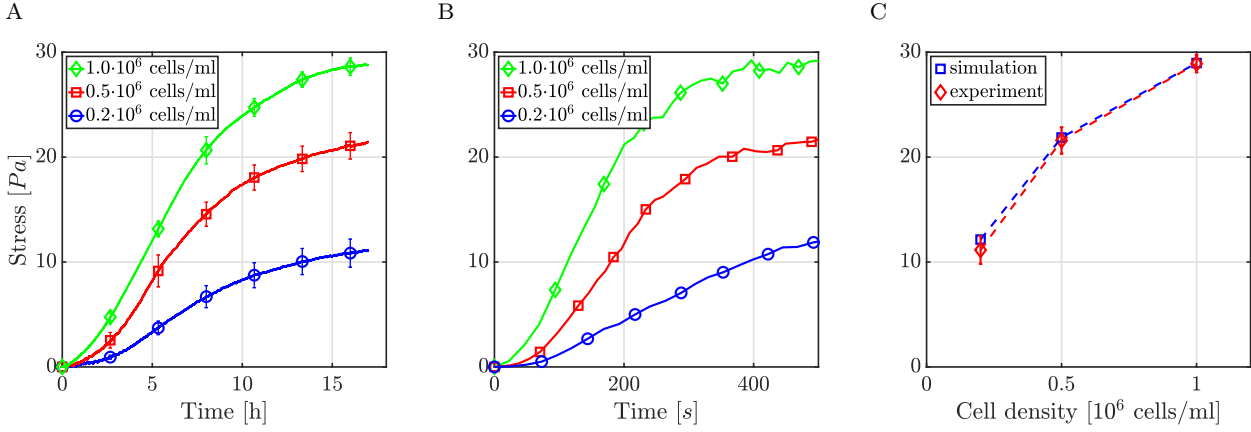### 3.3.2 Variation of collagen concentration

It is well-known that interactions between cells and their environment crucially depend on the stiffness of the environment. This holds in particular for the proliferation, survival, migration, and differentiation of cells (Wang et al., 2012; Nguyen et al., 2018; Balcioglu et al., 2020). A simple way of testing the impact of stiffness on cellular behavior in tissue culture studies is to change the collagen concentration of the tested gels (Hall et al., 2016; Joshi et al., 2018; Alcaraz et al., 2011; Miroshnikova et al., 2011). As shown in Fig. 8 A, tissue culture studies with a cell density of $0.5 \cdot 10^6$ cells/ml revealed that the cell-mediated first Piola-Kirchhoff stress increases in collagen gels with the collagen concentration (Eichinger et al., 2020; Delvoye et al., 1991). This behavior is both qualitatively and quantitatively reproduced well by our simulations as shown in Fig. 8 B. Interestingly, both experiments and simulations exhibit a nearly linear relation (with a slope of $\sim 9/2$) between collagen concentration and the homeostatic stress (Fig. 8 C). Moreover, the slope of the increase of stress up to the homeostatic stress was largely independent of the collagen concentration compared to the cell density in both the experiments and our simulations. We know from our simulations that an increased fiber density in case of higher collagen concentrations in combination with a constant distance between integrin binding spots on fibers of $50nm$ (López-García et al., 2010)

leads to more cell-matrix links per cell over time (data not shown) even when only the mechanisms presented in Section 2 are considered. If one assumes that cells stress fiber after fiber up to a certain level, this process takes longer if more fibers are present and can explain the observed nearly linear relationship between homeostatic stress and collagen concentration as well as the similar initial slope for all three collagen concentrations.

3.4 Residual matrix tension

Mechanical homeostasis in soft tissues is closely linked to growth (changes in mass) and remodeling (changes in microstructure) (Cyron and Humphrey, 2017). In particular, a reorganization of the microstructure of tissues includes a change in the mechanical links between tissue fibers and of the constituent-specific natural (stress-free) configurations. Experimental studies have revealed that remodeling of collagen gels induced by cellular forces is time-dependent and inelastic (Kim et al., 2017; Ban et al., 2018). Recent computational work suggested that the inelastic nature of cell-mediated remodeling is induced by force-dependent breaking of weak inter-fiber connections followed by the formation of bonds in new configurations leading to altered connections between tissue fibers (Kim et al., 2017; Ban et al., 2019; Nam et al., 2016; Cao et al., 2017) (Fig. 9 A). This implies that after cell-mediated remodeling, a part of the matrix tension remains in the tissue even after the elimination of all active cellular forces (e.g. by disrupting the actomyosin apparatus via addition of cytochalasin D or by cell lysis). This part is often referred to as residual matrix tension (RMT) (Simon et al., 2014; Marenzana et al., 2006).

To date, our quantitative understanding of how an altered state of the matrix is entrenched during remodeling and how RMT develops is limited. Even the exact kind of cross-linking which occurs when matrix tension is entrenched is unknown. An inelastic change of the stress-free configuration of the tissue could emerge from newly formed, transient bonds between collagen fibers (such as hydrogen bonds or van der Waals forces) as a result of fiber accumulation in the surroundings of contractile cells (Kim et al., 2017; Ban et al., 2018). However, RMT could also be entrenched by cells producing covalent cross-links via the actions of tissue transglutaminase or lysyl oxidase, which can also form new bonds between deformed matrix fibers. The impact of these enzymes on matrix remodeling has been shown experimentally in free-floating collagen gels (Simon et al., 2014). To study RMT, we simulated the experimental protocol presented in Marenzana et al. (2006) and eliminated active cellular forces from the simulated sys-

A

B

C

Fig. 6 For a collagen concentration of 1.5mg/ml, we compare the development of the first Piola-Kirchhoff stress in (A) experiments (Eichinger et al., 2020) and (B) simulations. A good semi-quantitative agreement of the expected cell-mediated steady state with non-zero tension (last data points of (A) and (B)) is observed (C), however, also a significant difference of the time scales.

A

B

C
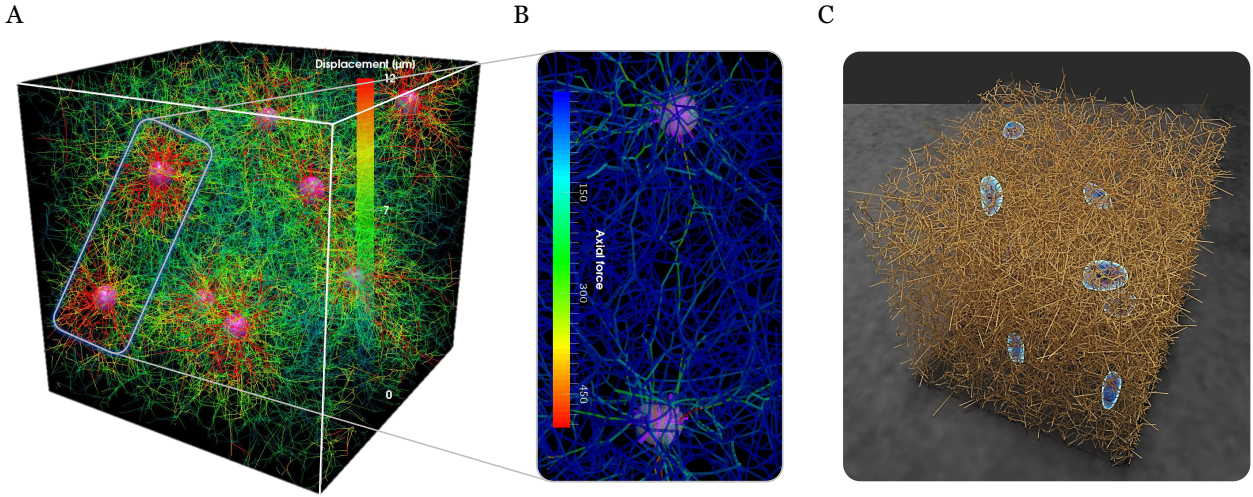
Fig. 7 Cells mechanically interact with surrounding matrix fibers. (A) Cells attach to nearby fibers, contract and thereby deform the matrix. The simulated, cell-mediated matrix displacements are in a realistic range when compared to experimental data (Notbohm et al., 2015; Malandrino et al., 2019). (B) Contracting cells can mechanically interact with other cells over a distance of several cell diameters via long-range mechanical signaling through matrix fibers, a phenomenon observed also in experiments (Kim et al., 2017; Ma et al., 2013; Shi et al., 2013; Baker et al., 2015; Mann et al., 2019). (C) Cells, visualized with reconstructed cell membrane around stress fibers, develop different shapes when pulling on the ECM.

tem in the homeostatic state by dissolving all existing cell-ECM bonds at a certain time (by setting $k_{on}^{c-f} = 0$, which led to a rapid dissolution of the remaining bonds). We then tracked tension over time in the RVE.

We first studied RMT in a purely covalently cross-linked network, implying that all existing bonds between fibers remained stable and no new bonds were formed during the simulation. After deactivating active cellular forces, we observed a (viscoelastic) decline of tension to zero in the RVE (Fig. 9 B bottom curve). This finding suggested that networks that lack the ability to form new, at least temporary stable, bonds cannot entrench a residual tension in the matrix, which

was however shown in the aforementioned experimental studies (Simon et al., 2014; Marenzana et al., 2006).

In a second step, transient linkers (which could, for example, be interpreted as un-bonded, freely floating collagen molecules or hydrogen bonds) were allowed to form between fiber-to-fiber binding spots with a certain on-rate k_{on}^{f-f}; they were able to be dissolved with a certain off-rate k_{off}^{f-f}. If two binding spots resided at some point in close proximity to two nearby fibers, a new, initially tension-free bond was formed according to Eq. (2). We found that introduction of newly formed, transient bonds enables the entrenchment of matrix remodeling and thus some RMT (Fig. 9 B, $k_{off}^{f-f} = 1.0e^{-04} \ s^{-1}$, $k_{off}^{f-f} = 3.0e^{-04} \ s^{-1}$, $k_{off}^{f-f} = 1.0e^{-03} \ s^{-1}$)
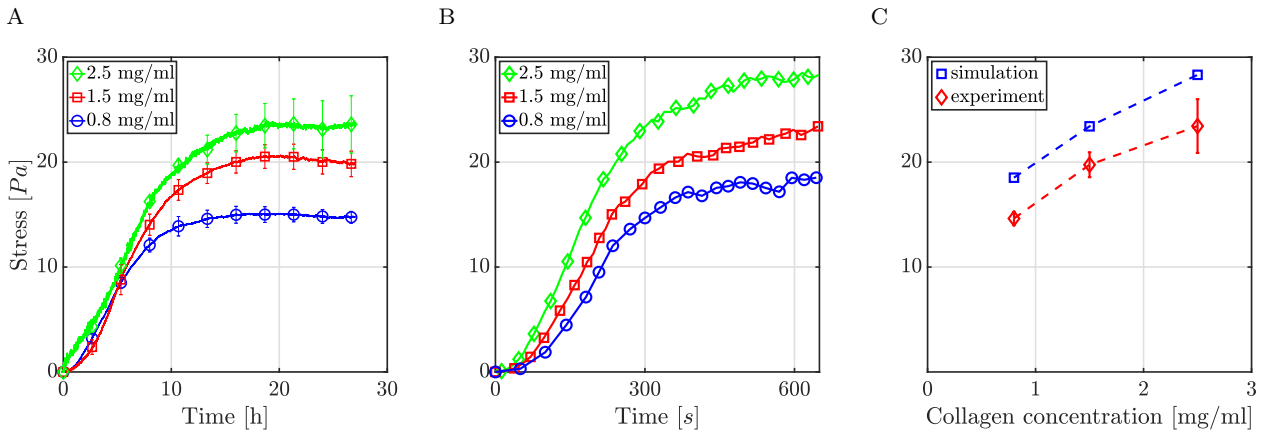
Fig. 8 Mechanical homeostasis for a cell concentration of $0.5 \cdot 10^6$ cells/ml and different collagen concentrations in (A) experiments (Eichinger et al., 2020) and (B) our simulations. (C) In both cases the relation between homeostatic first Piola-Kirchoff stress (last data points were taken respectively) and collagen concentration is approximately linear.

at least for a prolonged period. The transient nature of the cross-links between the fibers resulted, however, in a slow decrease of RMT over time. This decrease happened faster, the higher the off-rate k_{off}^{f-f} (Fig. 9 B). If k_{off}^{f-f} was chosen above a certain threshold, we did not observe any RMT.

In a third study, we allowed covalent cross-linker molecules to form between two nearby collagen fibers when they were within a certain distance to each other and Eq. (2) was fulfilled. By setting $k_{off}^{f-f} = 0$, a newly set bond could not be dissolved and was therefore covalent (permanent). In this case, we observed a substantial RMT that apparently did not decrease over time (Fig. 9 B, $k_{off}^{f-f} = 0.0 \ s^{-1}$).

It thus appears that both transient and covalent cross-links play roles in inelastic matrix remodeling. Our study suggests that RMT crucially depends on the ability of cells to entrench the deformation they impose on their neighborhood by covalent, permanent cross-links. Such a permanent entrenchment appears energetically favorable because it releases cells from the necessity of maintaining matrix tension over prolonged periods by active contractile forces, which consume considerable energy.

4 Conclusion

To date, our understanding of the governing principles of mechanical homeostasis in soft tissues on short time spans especially on the scale of individual cells remains limited (Eichinger et al., 2021). To address some of the many open questions in this area, we developed a novel computational framework for modeling cell-ECM interactions in three-dimensional RVEs of soft tissues. Our computational framework generates random fiber networks whose geometric characteristics resemble those

of actual collagen type I gels, that is, they exhibit a similar distribution of valency, free-fiber length, and orientation correlation (direction cosine) between adjacent fibers. These microstructural characteristics have been shown to be the primary determinants of the mechanical properties of fiber networks (Davoodi-Kermani et al., 2021). To model the mechanics of the collagen fibers in the network, our framework discretizes these fibers with geometrically exact nonlinear beam finite elements, which were shown in Section 3 to reproduce the elastic properties of collagen fiber networks. Our framework enables efficient parallel computing and can thus be used to simulate RVEs of tissues with realistic collagen concentrations and cell densities.

The physical interactions of cells with surrounding fibers through stress fibers in the cytoskeleton and transmembrane proteins (integrins) are modeled by contractile elastic springs whose binding and unbinding dynamics closely resemble the situation in focal adhesions. We used the non-trivial, experimentally determined relations of both cell density and collagen concentration to the homeostatic stress to show that the mechanisms accounted for in our computational framework are sufficient to capture theses relationships. We also demonstrated how our framework can help to (quantitatively) examine the micromechanical foundations of inelastic cell-mediated matrix remodeling and RMT, which persists in the tissue even after active cellular forces have been removed.

Despite its advantages and broad experimental foundation, the proposed computational framework has some limitations that remain to be addressed. First, our model does not yet capture mass turnover, that is, the deposition and degradation of fibers, which are assumed to be crucial for mechanical homeostasis on long time scales (Cyron and Humphrey, 2017; Humphrey and Ra-

A

B
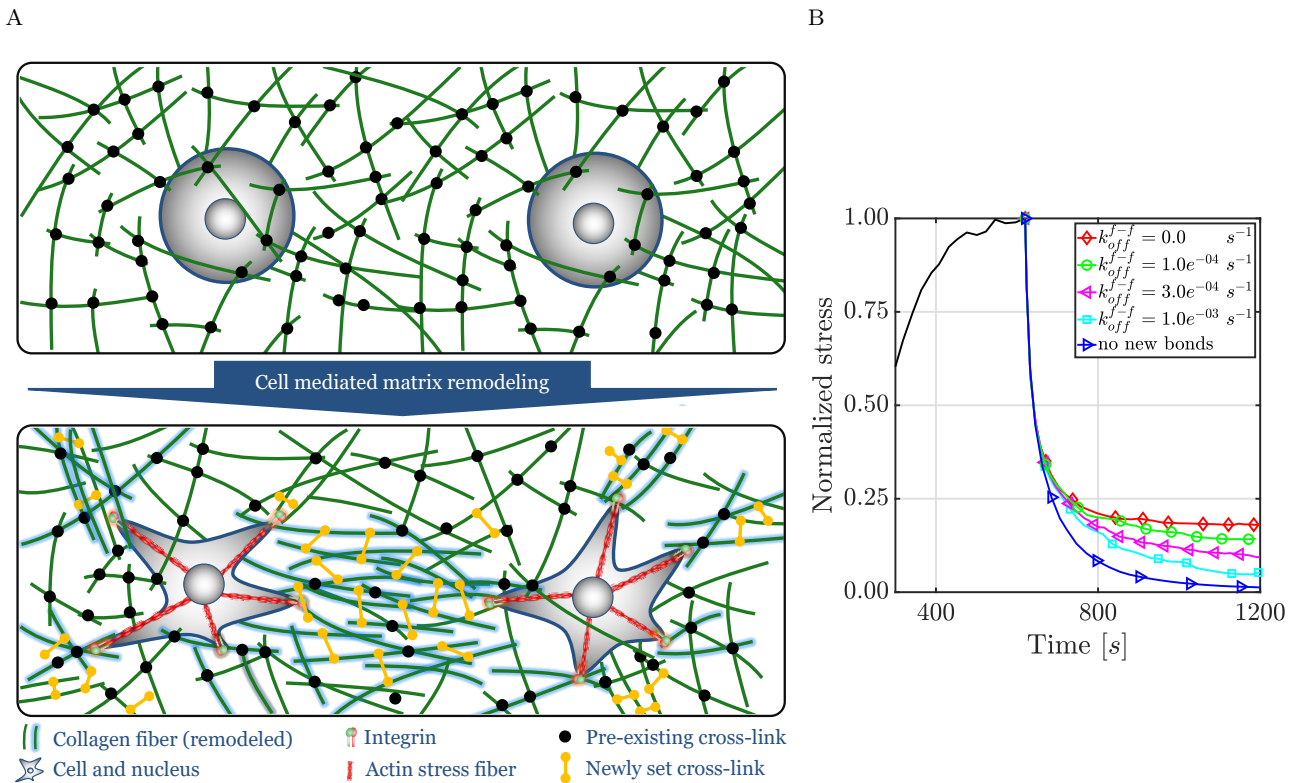
Fig. 9 (A) Cells actively remodel their surroundings, reorganizing the network and establishing new cross-links between its fibers. This way, cell-mediated tension can be entrenched in the network. (B) When removing active cellular forces suddenly, the matrix tension quickly drops. However, if cells have entrenched their reorganization of the network structure by permanent (covalent) cross-links (with $k_{off}^{f-f} = 0.0$), a residual tension persists in the network. By setting transient cross-links with a sufficiently low off-rate, the cells can ensure an RMT at least over the periods considered.

jagopal, 2002; Ambrosi et al., 2011; Cyron et al., 2016; Braeu et al., 2017). Moreover, it models integrins but not other proteins playing a key role in the interactions between cells and surrounding matrix such as talin and vinculin (Ziegler et al., 2008; Das et al., 2014; Yao et al., 2014, 2016; Austen et al., 2015; Truong et al., 2015; Davidson et al., 2015; Zhu et al., 2016; Ringer et al., 2017; Grashoff et al., 2010; Carisey et al., 2013; Dumbauld et al., 2013). Also the model of cellular contractility is simplistic and should be endowed with additional biological details (Mogilner and Oster, 2003; Murtada et al., 2010, 2012). Finally, we did not consider contact forces between fibers or between cells and fibers (assuming that cells and fibers mainly interact via integrins). While this reduces the computational cost substantially, a comprehensive incorporation of contact mechanics could also help to make our computational framework more realistic.

An important field of application for our computational framework will be *in silico* studies in which one can test step by step which additional features have to be incorporated in the framework to capture more and more phenomena observed *in vitro* and *in vivo*. Like

this, it may contribute to uncover the micromechanical foundations of mechanical homeostasis on the level of individual cells and fibers and help to understand how these microscopic processes lead to what we call mechanical homeostasis on the macroscale.

Appendix

A1 Construction of random fiber networks by simulated annealing

In this appendix, we present the computational details of the algorithm we used for constructing network RVEs as an input for our simulations. Our algorithm closely follows the approach of Lindström et al. (2010), using the stochastic optimization method of simulated annealing for constructing random heterogeneous media introduced by Yeong and Torquato (1998). Thereby, one assumes that the geometry of a fiber network can be characterized by some descriptors $\boldsymbol{x}_i$, with $i \in \{l, c\}$, in our case representing the fiber length and the direction cosine, respectively. These descriptors can be understood as random variables taking on specific values at certain nodes or fibers and characterize the network microstructure. The descriptors are assumed to follow some statistical distribution $P^i(x_i)$ across the different fibers and nodes. These distributions can be determined, for example, from confocal microscopy images of real networks, see also Fig. A1. According to Lindström et al. (2010), this yields for collagen type-I networks

$$P^l(l) = \frac{1}{l\sigma\sqrt{2\pi}} \exp\left(-\frac{[\mu - \ln(l)]^2}{2\sigma^2}\right), \qquad (A1)$$

where l denotes the fiber length normalized by $(N/V_{RVE})^{\frac{1}{3}}$, with V_{RVE} being the volume of the RVE and N representing the total number of network nodes in it. The parameters σ and μ denote a standard deviation and mean value that may vary from network to network. Typical parameters are given in Table A1. The cumulative probability distribution associated with $P^l(l)$ is given by

$$C^l(l) = \frac{1}{2} + \frac{1}{2}\,\mathrm{erf}\left(\frac{\ln(x) - \mu}{\sqrt{2}\sigma}\right) \qquad (A2)$$

and will be used below in Eq. (A7).

The distribution of the direction cosine β of fibers adjacent to the same node has been described by Lindström et al. (2010) by a truncated power series

$$P^c(\beta) = \sum_{k=1}^{3} b_k\,(1 - \beta)^{2k-1}, \qquad (A3)$$

with the associated cumulative distribution function

$$C^c(\beta) = 1 + \sum_{k=1}^{3} -\frac{b_k}{2k}\,(1 - \beta)^{2k-1}. \qquad (A4)$$

Again, typical values for the parameters b_k are given in Table A1. To describe the valency distribution of the

networks, we relied on the data reported in Nan et al. (2018).

Our target was to construct artificial random fiber networks as an input for our simulations whose descriptor distributions matched the ones defined above. To this end, we started from some random initial network. This network was then evolved in a number of discrete random steps according to the concept of simulated annealing (Kirkpatrick et al., 1983), until the descriptor distributions matched the desired target distributions.

To define the random initial configuration, we started by generating networks based on three-dimensional Voronoi tesselations (Rycroft, 2009) with periodic boundary conditions applied in all directions. Subsequently, we randomly removed and added fibers until the valency distribution matched its target distribution. Only then we started the actual simulated annealing, where only fiber length and direction cosine distributions still had to be matched to their target distributions. The simulated annealing was performed following the concept introduced by Kirkpatrick et al. (1983). The idea is to iteratively select random nodes in the network and apply random displacements to them (Fig. 1 B). Like this, the length of all fibers attached to the respective node and the angles between these fibers change. Importantly, only movements of nodes are accepted which do not lead to fiber lengths larger than one third of the smallest edge length of the RVE to ensure that it stays *representative*. Note, that a movement of a node does not affect its connectivity, which ensures that the initially created valency distribution remains unaffected during the whole simulated annealing.

For stochastic optimization according to the simulated annealing concept, it is helpful to define an objective (energy-type) function E

$$E = w_l \cdot E^l + w_c \cdot E^c. \qquad (A5)$$

where the E^l and E^c become minimal if the length and direction cosine distribution exactly match their target distributions and where the $w_i > 0$ are weights that can be adapted to tune the importance of a specific distribution function. Having defined the objective function E, simulated annealing can be understood as a stochastic minimization of E. Once the minimum is found, E^l and E^c must be minimal and thus the length and direction cosine distributions match their target distributions. To perform a stochastic minimization of E, a Metropolis algorithm is applied during the simulated annealing. It consists of a sequence of random steps. For each of these steps the associated change of E is computed, that is, ΔE. Then, the step is actually performed only with a likelihood

A

B

C
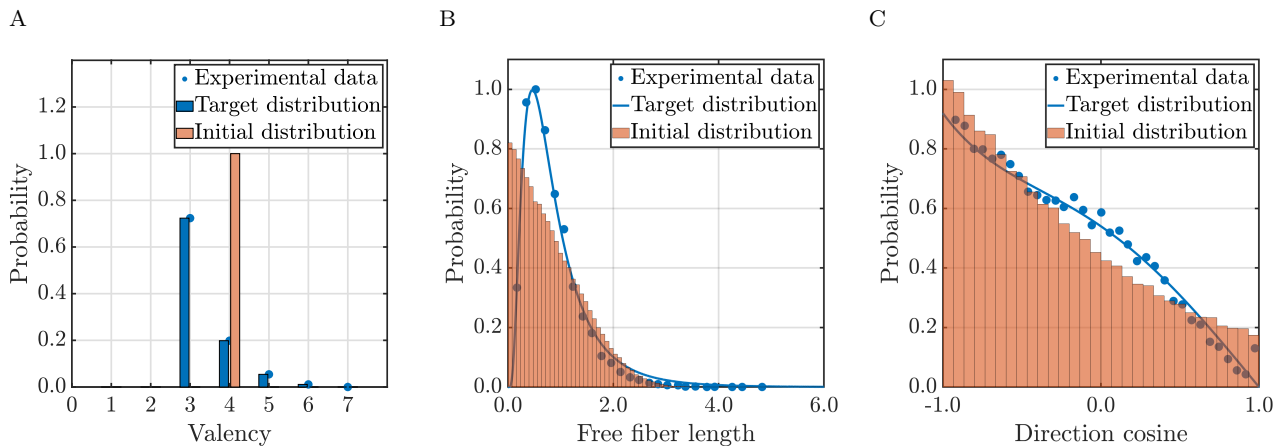
Fig. A1 Random initial descriptor distributions in a network generated by Voronoi tesselation vs. target distributions fitted by Lindström et al. (2010) and Nan et al. (2018) to experimental data (collagen concentration $2.5mg/ml$). Simulated annealing alters the initial network until its descriptor distributions match the required target distributions.

Table A1 Parameters for length, valency and cosine distribution functions according to Lindström et al. (2010) and parameters used for simulated annealing process

Parameter	Description	Value [-]
w_l	weight for free-fiber length distribution in Eq. (A5)	1.0
w_c	weight for direction cosine distribution in Eq. (A5)	1.0
μ	mean in Eq. (A1) and (A2)	-0.3000
σ	standard deviation in Eq. (A1) and (A2)	0.6008
b_1	parameter for truncated power series in Eq. (A3) and (A4)	0.6467
b_2	parameter for truncated power series in Eq. (A3) and (A4)	-0.1267
b_3	parameter for truncated power series in Eq. (A3) and (A4)	0.0200
b_l	number of bins for free-fiber length distribution in Eq. (A7)	1000
b_c	number of bins for direction cosine distribution in Eq. (A7)	1000
T_0	initial temperature	0.05
-	resulting average node valency of constructed networks	3.3

$$p_{accept}(\Delta E) = \begin{cases} 1, & \Delta E \leq 0 \\ \exp(-\frac{\Delta E}{T}), & \Delta E > 0, \end{cases} \qquad (A6)$$

where T denotes a temperature-like parameter. In our simulated annealing, we slowly decreased T as the number random steps increased, using at the annealing step k the value $T = 0.95^k \cdot T_0$ (according to Nan et al. (2018)). We chose T_0 such that the probability for accepting a random step with $\Delta E > 0$ was approximately 0.5 in the beginning. In practice, the simulated annealing was stopped if either the total energy of the system was below a predefined threshold or a maximal number of iterations was reached.

Remark A1: It is worth noting, that for constructing RVEs with different collagen concentrations, we assumed the same target distributions for the valency, direction cosine and normalized fiber length. Only the normalization factor of the fiber length was changed. Moreover, an increased collagen concentration automat-

ically also implies a higher number N of network nodes in the RVE.

Remark A2: While there exists a variety of simple and obvious choices for the E^i in (A5), these mostly suffer from a computational cost on the order of $\mathcal{O}(n_i)$ with n_i being the number of instances of a descriptor. This makes the generation of large random networks practically infeasible. To overcome this problem, we adopted the idea of Lindström et al. (2010) to use a binning algorithm and define the E^i as Cramer-von Mises test statistics, which reduces the computational cost to the order of $\mathcal{O}(b)$ with b being the number of bins. To this end, we divided the range of $\boldsymbol{x_i}$ in b_i disjoint intervals (bins) and assigned each instance of a descriptor at a fiber or node of a random network to its associated bin. The resulting histogram is a discrete approximation of $P^i(x_i)$. The center of the j-th bin is denoted by x_{ij}. The number of instances of descriptor x_i assigned to the j-th bin is m_{ij}. The Cramer-von

Mises test statistics can then be computed as

$$E^i = \frac{1}{n_i^2} \sum_{j=1}^{b_i} m_{ij} \left[\frac{1}{6}(m_{ij}+1)(6S_{ij}+2m_{ij}+1) + S_{ij}^2 \right]$$
$$(A7)$$

with $S_{ij} = M_{i(j-1)} - nC^i(x_{ij}) - \frac{1}{2}$, $M_{ij} = \sum_{k=1}^{j} m_{ik}$, and C^i the cumulative distribution of x_i.

A2 Boundary conditions

In this appendix, we briefly summarize how we applied fully periodic boundary conditions to our simulation domains. Let these domains be cuboids with edge length L_i in the i-th coordinate direction. In a fully periodic network, the part of a fiber sticking out across one periodic boundary must have a counterpart entering the RVE at the opposite side (Fig. A2 A). One can interpret the element part sticking out of the domain at one boundary and the element part entering the RVE at the opposite boundary also as a fictitious single element (Fig. A2 B, state II) cut into two parts (Fig. A2 B, state I). Thereby, state I as delineated in Fig. A2 B can be used to evaluate interactions with other fibers or cells, and state II for evaluating strains and stresses on element level. If the element is cutting through a boundary in the i-th coordinate direction, the i-th coordinate of the nodal positions in state I and state II are shifted by L_i relative to each other. Importantly, only the translational degrees of freedom of the beam finite element nodes are affected by the periodic boundaries, rotational degrees of freedom remain unaffected.

It is a major challenge to impose periodic Dirichlet boundary conditions on fiber networks in a manner that is fully periodic. Note that most of the literature (Stein et al., 2010; Lee et al., 2014; Humphries et al., 2018; Abhilash et al., 2014; Burkel et al., 2018; Ban et al., 2018; Liang et al., 2016; Ban et al., 2019) bypasses this difficulty by fixing nodes on or close to the periodic boundary in a manner that actually unfortunately cannot ensure periodicity in a rigorous manner. To overcome this deficiency, we used the following approach. Dirichlet boundary conditions of RVE can be represented by normal or shear strains. These strains can be converted into a relative displacement of opposite periodic boundaries by components Δd_j in the j-th coordinate direction. We accounted for this displacement by stretching (Fig. A2 C) or shearing (Fig. A2 D) the RVE as a whole. The nodal positions in state I and II were then no longer converted into each other in the above described simple manner, that is, by a relative shift by L_i in the i-the direction. Rather all coordinates

of the nodal positions were additionally shifted relative to each other by the components Δd_j. Note that this approach can account also for complex multi-axial loading by applying the described procedure at all periodic boundaries. Moreover, this approach can account also for large strains.

A3 Search algorithm and parallel computing

In this appendix we describe how we ensured efficient parallel computing for the presented modeling framework in our in-house finite element solver BACI (BACI, 2021). Parallelization of the finite element discretization of the fibers can be handled with standard libraries such as the Trilinos libraries that formed the basis of our in-house code. Therefore, we focus herein on the parallelization of cell-fiber interactions and chemical bonds between fibers. Both require search algorithms to identify cell-fiber or fiber-fiber pairs that may interact at a certain point in time. We implemented a search algorithm based on a geometrical decomposition of the computational domain (RVE) in uniform cubic containers. For simplicity, these were aligned with the axes of our coordinate system (see Fig. A3). Cells and finite beam elements are assigned to all containers with which they overlap. We chose the minimal size of the containers such that all possible interaction partners were certainly located within one layer of neighboring containers. Hence, evaluating the possible interactions of a single cell or beam finite element simply required searching within one layer of containers around the containers to which the cell or element was assigned.

The content of the containers had to be updated over time as cells and matrix fibers moved during our simulations. Depending on the time step size of our simulations, container size and effective physical interaction distance, it was feasible to update our containers only every n-th time step.

The potentially large domain considered in our simulations typically required a distribution of the above described containers on several processors. To this end, each processor was assigned a set of containers forming a connected sub-domain. In addition to these containers, each processor was also provided full information about one layer of so-called ghost containers surrounding its specific sub-domain (Fig. A3 B). The computational cost of sharing the information about ghost containers was negligible compared to the the overall computational cost of our simulations.

To always allow an effective search algorithm based on a rectangular Cartesian domain, we used a coordinate transformation to the undeformed domain in
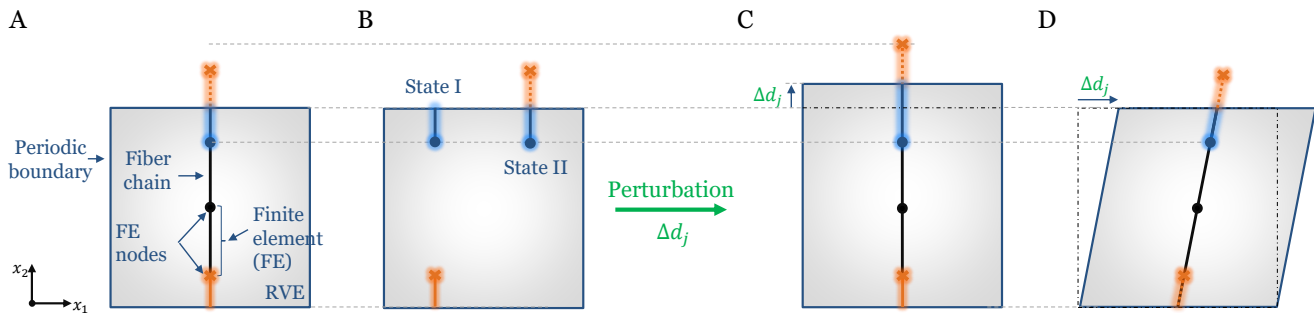
Fig. A2 Illustration of periodic boundary conditions using the example of a single fiber in the network: (A) any fraction of an element sticking out of a periodic boundary must have a counterpart entering at the opposite side; (B) both element fractions together define what is physically present within the RVE (state I). To compute strains and stresses in both element fractions, it is convenient to use a fictitious state II (shifted rightwards in the figure for illustration purposes only), which represents the part of the cut element within the simulated RVE and the part located in an adjacent domain periodically continuing the RVE; (C) application of fully periodic normal strain boundary condition in vertical direction; (D) application of fully periodic shear strain boundary condition in the drawing plane.
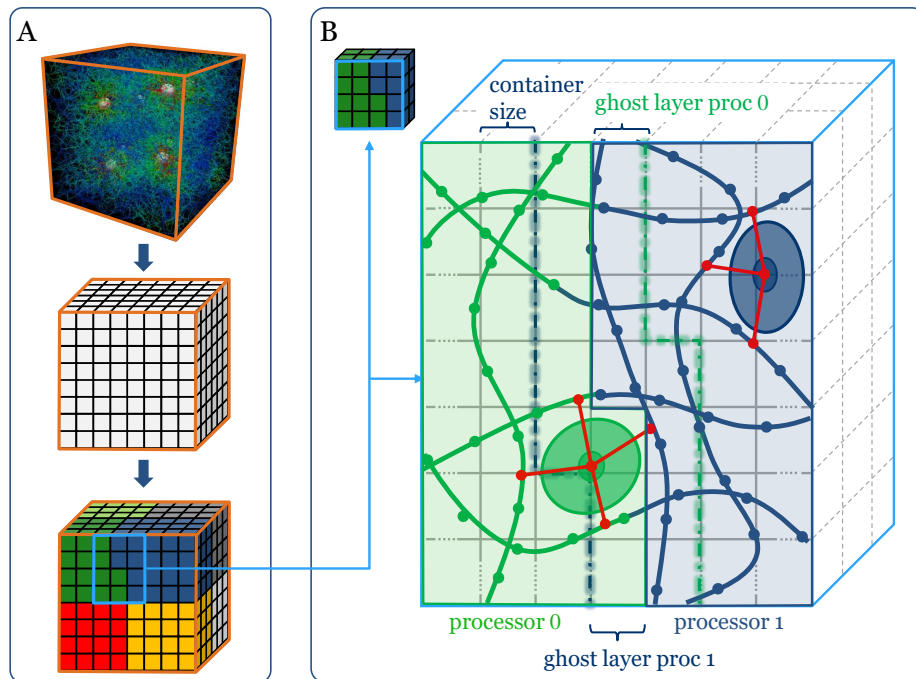
Fig. A3 (A) Our computational domain (top) was divided into a large number of cubic containers (middle). Sets of numerous such containers (highlighted by different colors, bottom) were distributed to different processors. (B) All fibers discretized by beam finite elements as well as all cells were assigned to all containers with which they overlapped. Each processor was provided not only information about its own containers but also about a layer of ghost containers with whose elements the elements in its own container may interact.

case boundary conditions imposing a deformation of the computational domain.

It is worth mentioning that in our parallelization framework no data (except some uncritical parameters such as the current time step) need be stored fully redundantly on all processors, which would drastically limit the problem sizes.

A4 Simulation parameters

Table A2 List of parameters and default values of computational model

Parameter	Description	Value	Reference
a_1	Integrin catch-slip bond parameter	2.2	to fit data of Kong et al. (2009)
b_1	Integrin catch-slip bond parameter	29.9	to fit data of Kong et al. (2009)
c_1	Integrin catch-slip bond parameter	8.4	to fit data of Kong et al. (2009)
a_1	Integrin catch-slip bond parameter	1.2	to fit data of Kong et al. (2009)
b_2	Integrin catch-slip bond parameter	16.2	to fit data of Kong et al. (2009)
c_3	Integrin catch-slip bond parameter	37.8	to fit data of Kong et al. (2009)
R	Cell radius	$12~\mu m$	typical value
ΔR	Linking range around cell	$\pm 3\mu m$	-
D_f	Diameter of collagen fibers	$180~nm$	Van Der Rijt et al. (2006)
E_f	Young's Modulus of collagen fibers	$1.1 MPa$	Jansen et al. (2018)
$\dot{c}$	Contraction rate stress fiber	$0.1\frac{\mu m}{s}$	Choquet et al. (1997) Moore et al. (2010)
$k_B T$	Thermal energy	$4.28 \cdot 10^{-3}~aJ$	at 37℃
L_i	RVE edge length in i-th coordinate direction	$245\mu m$	-
k_{on}^{f-f}	Chemical association rate for fiber linker	$0.0001 s^{-1}$	-
k_{off}^{f-f}	Chemical dissociation rate for fiber linker	$0.0001 s^{-1}$	-
Δx	Bell parameter	$0.5 nm$	-
$N_{FA,max}$	Maximal number of focal adhesion per cell	65	Horzum et al. (2014) Kim and Wirtz (2013) Mason et al. (2019)
$N_{i,FA,max}$	Maximal number of integrins per focal adhesion	1000	Wiseman (2004) Elosegui-Artola et al. (2014)
$N_{i,ic,max}$	Maximal number of integrins per cluster	20	Changede et al. (2015) Cheng et al. (2020)
k_{on}^{c-f}	Chemical association rate for integrin	$0.1 s^{-1}$	slightly modified Zhu et al. (2016)
d^{i-f}	Distance between binding spots for integrin-fiber links	$50 nm$	López-García et al. (2010)

References

Abhilash, A. S., Baker, B. M., Trappmann, B., Chen, C. S., and Shenoy, V. B. (2014). Remodeling of fibrous extracellular matrices by contractile cells: Predictions from discrete fiber network simulations. *Biophys. J.*, 107(8):1829–1840.

Alcaraz, J., Mori, H., Ghajar, C. M., Brownfield, D., Galgoczy, R., and Bissell, M. J. (2011). Collective epithelial cell invasion overcomes mechanical barriers of collagenous extracellular matrix by a narrow tube-like geometry and MMP14-dependent local softening. *Integr. Biol.*, 3(12):1153–1166.

Ambrosi, D., Ateshian, G., Arruda, E., Cowin, S., Dumais, J., Goriely, A., Holzapfel, G., Humphrey, J., Kemkemer, R., Kuhl, E., Olberding, J., Taber, L., and Garikipati, K. (2011). Perspectives on biological growth and remodeling. *J. Mech. Phys. Solids*, 59(4):863–883.

Austen, K., Ringer, P., Mehlich, A., Chrostek-grashoff, A., Kluger, C., Klingner, C., Sabass, B., Zent, R., Rief, M., and Grashoff, C. (2015). Extracellular rigidity sensing by talin isoform-specific mechanical linkages. *Nat. Cell Biol.*, 17(12):1597–1606.

BACI (2021). BACI: A Comphrehensive Multi-Physics Simulation Framework.

Baker, B. M. and Chen, C. S. (2012). Deconstructing the third dimension-how 3D culture microenvironments alter cellular cues. *J. Cell Sci.*, 125(13):3015–3024.

Baker, B. M., Trappmann, B., Wang, W. Y., Sakar, M. S., Kim, I. L., Shenoy, V. B., Burdick, J. A., and Chen, C. S. (2015). Cell-mediated fibre recruitment drives extracellular matrix mechanosensing in engineered fibrillar microenvironments. *Nat. Mater.*, 14(12):1262–1268.

Balcioglu, H. E., Balasubramaniam, L., Stirbat, T. V., Doss, B. L., Fardin, M. A., Mège, R. M., and Ladoux, B. (2020). A subtle relationship between substrate stiffness and collective migration of cell clusters. *Soft Matter*, 16(7):1825–1839.

Ban, E., Franklin, J. M., Nam, S., Smith, L. R., Wang, H., Wells, R. G., Chaudhuri, O., Liphardt, J. T., and Shenoy, V. B. (2018). Mechanisms of Plastic Deformation in Collagen Networks Induced by Cellular Forces. *Biophys. J.*, 114(2):450–461.

Ban, E., Wang, H., Franklin, J. M., Liphardt, J. T., Janmey, P. A., and Shenoy, V. B. (2019). Strong triaxial coupling and anomalous Poisson effect in collagen networks. *Proc. Natl. Acad. Sci.*, page 201815659.

Bates, R. C., Lincz, L. F., and Burns, G. F. (1995). Involvement of integrins in cell survival. *Cancer Metastasis Rev.*, 14(3):191–203.

Bell, G. I. (1980). Theoretical models for the specific adhesion of cells to cells or to surfaces. *Adv. Appl. Probab.*, 12(03):566–567.

Bircher, K., Zündel, M., Pensalfini, M., Ehret, A. E., and Mazza, E. (2019). Tear resistance of soft collagenous tissues. *Nat. Commun.*, 10(1):1–13.

Bonnans, C., Chou, J., and Werb, Z. (2014). Remodelling the extracellular matrix in development and disease. *Nat. Rev. Mol. Cell Biol.*, 15(12):786–801.

Braeu, F. A., Seitz, A., Aydin, R. C., and Cyron, C. J. (2017). Homogenized constrained mixture models for anisotropic volumetric growth and remodeling. *Biomech. Model. Mechanobiol.*, 16(3):889–906.

Broedersz, C. P., Mao, X., Lubensky, T. C., and Mackintosh, F. C. (2011). Criticality and isostaticity in fibre networks. *Nat. Phys.*, 7(12):983–988.

Brown, R. A., Prajapati, R., McGrouther, D. A., Yannas, I. V., and Eastwood, M. (1998). Tensional homeostasis in dermal fibroblasts: Mechanical responses to mechanical loading in three-dimensional substrates. *J. Cell. Physiol.*, 175(3):323–332.

Brown, R. A., Sethi, K. K., Gwanmesia, I., Raemdonck, D., Eastwood, M., and Mudera, V. (2002). Enhanced fibroblast contraction of 3D collagen lattices and integrin expression by TGF-β1 and -β3: Mechanoregulatory growth factors? *Exp. Cell Res.*, 274(2):310–322.

Burkel, B., Proestaki, M., Tyznik, S., and Notbohm, J. (2018). Heterogeneity and nonaffinity of cell-induced matrix displacements. *Phys. Rev. E*, 98(5):1–13.

Campbell, B. H., Clark, W. W., and Wang, J. H. C. (2003). A multi-station culture force monitor system to study cellular contractility. *J. Biomech.*, 36(1):137–140.

Cao, X., Ban, E., Baker, B. M., Lin, Y., Burdick, J. A., Chen, C. S., and Shenoy, V. B. (2017). Multiscale model predicts increasing focal adhesion size with decreasing stiffness in fibrous matrices. *Proc. Natl. Acad. Sci.*, 114(23):E4549—-E4555.

Carisey, A., Tsang, R., Greiner, A. M., Nijenhuis, N., Heath, N., Nazgiewicz, A., Kemkemer, R., Derby, B., Spatz, J., and Ballestrem, C. (2013). Vinculin regulates the recruitment and release of core focal adhesion proteins in a force-dependent manner. *Curr. Biol.*, 23(4):271–281.

Cavalcanti-Adam, E. A., Volberg, T., Micoulet, A., Kessler, H., Geiger, B., and Spatz, J. P. (2007). Cell Spreading and Focal Adhesion Dynamics Are Regulated by Spacing of Integrin Ligands. *Biophys. J.*, 92(8):2964–2974.

Changede, R., Xu, X., Margadant, F., and Sheetz, M. P. (2015). Nascent Integrin Adhesions Form on All Matrix Rigidities after Integrin Activation. *Dev. Cell*, 35(5):614–621.

Chatterjee, A. P. (2010). Nonuniform fiber networks and fiber-based composites: Pore size distributions and elastic moduli. *J. Appl. Phys.*, 108(6).

Cheng, B., Wan, W., Huang, G., Li, Y., Genin, G. M., Mofrad, M. R., Lu, T. J., Xu, F., and Lin, M. (2020). Nanoscale integrin cluster dynamics controls cellular mechanosensing via FAKY397 phosphorylation. *Sci. Adv.*, 6(10).

Chiquet, M., Gelman, L., Lutz, R., and Maier, S. (2009). From mechanotransduction to extracellular matrix gene expression in fibroblasts. *Biochim. Biophys. Acta - Mol. Cell Res.*, 1793(5):911–920.

Choquet, D., Felsenfeld, D. P., Sheetz, M. P., and Carolina, N. (1997). Extracellular Matrix Rigidity Causes Strengthening of Integrin – Cytoskeleton Linkages. *Cell*, 88(1):39–48.

Courderot-Masuyer, C. (2017). *Mechanical Properties of Fibroblasts*. Springer.

Cox, T. R. and Erler, J. T. (2011). Remodeling and homeostasis of the extracellular matrix: implications for fibrotic diseases and cancer. *Dis. Model. Mech.*, 4(2):165–178.

Cyron, C. and Wall, W. A. (2012). Numerical method for the simulation of the Brownian dynamics of rod-like microstructures with three-dimensional nonlinear beam elements. *Int. j. numer. method. biomed. eng.*, 90(April):1102–1119.

Cyron, C. J., Aydin, R. C., and Humphrey, J. D. (2016). A homogenized constrained mixture (and mechanical analog) model for growth and remodeling of soft tissue. *Biomech. Model. Mechanobiol.*, 15(6):1389–1403.

Cyron, C. J. and Humphrey, J. D. (2017). Growth and remodeling of load-bearing biological soft tissues. *Meccanica*, 52(3):645–664.

Cyron, C. J., Müller, K. W., Bausch, A. R., and Wall, W. A. (2013a). Micromechanical simulations of biopolymer networks with finite elements. *J. Comput. Phys.*, 244:236–251.

Cyron, C. J., Müller, K. W., Schmoller, K. M., Bausch, A. R., Wall, W. A., and Bruinsma, R. F. (2013b). Equilibrium phase diagram of semi-flexible polymer networks with linkers. *Epl*, 102(3).

Dahlmann-Noor, A. H., Martin-Martin, B., Eastwood, M., Khaw, P. T., and Bailly, M. (2007). Dynamic protrusive cell behaviour generates force and drives early matrix contraction by fibroblasts. *Exp. Cell Res.*, 313(20):4158–4169.

Das, M., Subbayya Ithychanda, S., Qin, J., and Plow, E. F. (2014). Mechanisms of talin-dependent integrin signaling and crosstalk. *Biochim. Biophys. Acta - Biomembr.*, 1838(2):579–588.

Davidson, M. W., Ruehland, S., Baird, M. A., Teo, S., Bate, N., Kanchanawong, P., Goh, W. I., Wang, Y.,

Goh, H., Critchley, D. R., and Liu, J. (2015). Talin determines the nanoscale architecture of focal adhesions. *Proc. Natl. Acad. Sci.*, 112(35):E4864–E4873.

Davoodi-Kermani, I., Schmitter, M., Eichinger, J. F., Aydin, R. C., and Cyron, C. J. (2021). Computational study of the geometric properties governing the linear mechanical behavior of fiber networks. *submitted.*

Delvoye, P., Wiliquet, P., Levêque, J.-L., Nusgens, B. V., and Lapière, C. M. (1991). Measurement of Mechanical Forces Generated by Skin Fibroblasts Embedded in a Three-Dimensional Collagen Gel.

Domaschke, S., Morel, A., Fortunato, G., and Ehret, A. E. (2019). Random auxetics from buckling fibre networks. *Nat. Commun.*, 10(1):1–8.

Domaschke, S., Morel, A., Kaufmann, R., Hofmann, J., Rossi, R. M., Mazza, E., Fortunato, G., and Ehret, A. E. (2020). Predicting the macroscopic response of electrospun membranes based on microstructure and single fibre properties. *J. Mech. Behav. Biomed. Mater.*, 104(January).

Dong, S., Huang, Z., Tang, L., Zhang, X., Zhang, Y., and Jiang, Y. (2017). A three-dimensional collagen-fiber network model of the extracellular matrix for the simulation of the mechanical behaviors and micro structures. *Comput. Methods Biomech. Biomed. Engin.*, 20(9):991–1003.

Dumbauld, D. W., Lee, T. T., Singh, A., Scrimgeour, J., Gersbach, C. A., Zamir, E. A., Fu, J., Chen, C. S., Curtis, J. E., and Craig, S. W. (2013). How vinculin regulates force transmission. *PNAS.*

Duval, K., Grover, H., Han, L. H., Mou, Y., Pegoraro, A. F., Fredberg, J., and Chen, Z. (2017). Modeling physiological events in 2D vs. 3D cell culture. *Physiology*, 32(4):266–277.

Eichinger, J. F., Haeusel, L. J., Paukner, D., Aydin, R. C., Humphrey, J. D., and Cyron, C. J. (2021). Mechanical homeostasis in tissue equivalents - a review. *Biomech. Model. Mechanobiol.*

Eichinger, J. F., Paukner, D., Szafron, J. M., Aydin, R. C., Humphrey, J. D., and Cyron, C. J. (2020). Computer-Controlled Biaxial Bioreactor for Investigating Cell-Mediated Homeostasis in Tissue Equivalents. *J. Biomech. Eng.*, 142(7):1–22.

Elosegui-Artola, A., Bazellières, E., Allen, M. D., Andreu, I., Oria, R., Sunyer, R., Gomm, J. J., Marshall, J. F., Jones, J. L., Trepat, X., and Roca-Cusachs, P. (2014). Rigidity sensing and adaptation through regulation of integrin types. *Nat. Mater.*, 13(6):631–637.

Ezra, D. G., Ellis, J. S., Beaconsfield, M., Collin, R., and Bailly, M. (2010). Changes in fibroblast mechanostat set point and mechanosensitivity: An adaptive response to mechanical stress in floppy eyelid syndrome. *Investig. Ophthalmol. Vis. Sci.*, 51(8):3853–3863.

Grashoff, C., Hoffman, B. D., Brenner, M. D., Zhou, R., Parsons, M., Yang, M. T., McLean, M. A., Sligar, S. G., Chen, C. S., Ha, T., and Schwartz, M. A. (2010). Measuring mechanical tension across vinculin reveals regulation of focal adhesion dynamics. *Nature*, 466(7303):263–266.

Grill, M. J., Eichinger, J. F., Koban, J., Meier, C., Lieleg, O., and Wall, W. A. (2020). Modeling and Simulation of the Hindered Mobility of Charged Particles in Biological Hydrogel. *Proc. R. Soc. A.*

Grimmer, P. and Notbohm, J. (2017). Displacement Propagation in Fibrous Networks Due to Local Contraction. *J. Biomech. Eng.*, 140(4):1–11.

Grinnell, F. and Petroll, W. M. (2010). Cell Motility and Mechanics in Three-Dimensional Collagen Matrices. *Annu. Rev. Cell Dev. Biol.*, 26(1):335–361.

Hall, M. S., Alisafaei, F., Ban, E., Feng, X., Hui, C.-Y., Shenoy, V. B., and Wu, M. (2016). Fibrous nonlinear elasticity enables positive mechanical feedback between cells and ECMs. *Proc. Natl. Acad. Sci.*, 113(49):14043–14048.

Heussinger, C. and Frey, E. (2007). Force distributions and force chains in random stiff fiber networks. *Eur. Phys. J. E*, 24(1):47–53.

Hippler, M., Weißenbruch, K., Richler, K., Lemma, E. D., Nakahata, M., Richter, B., Barner-kowollik, C., Takashima, Y., Harada, A., Blasco, E., Wegener, M., Tanaka, M., and Bastmeyer, M. (2020). Mechanical stimulation of single cells by reversible host-guest interactions in 3D microscaffolds. *Sci. Adv.*, 6(39).

Horzum, U., Ozdil, B., and Pesen-Okvur, D. (2014). Step-by-step quantitative analysis of focal adhesions. *MethodsX*, 1(1):56–59.

Hulmes, D. J. (1979). Quasi-hexagonal molecular packing in collagen fibrils.

Humphrey, J. D., Dufresne, E. R., and Schwartz, M. A. (2014). Mechanotransduction and extracellular matrix homeostasis. *Nat. Rev. Mol. Cell Biol.*, 15(12):802–812.

Humphrey, J. D. and Rajagopal, K. R. (2002). A constrained mixture model for growth and remodeling of soft tissues. *Math. Model. Methods Appl. Sci.*, 12(3):407–430.

Humphries, D., Grogan, J., and Gaffney, E. (2018). The mechanics of phantom Mikado networks. *J. Phys. Commun.*, 2(5):055015.

Humphries, D. L., Grogan, J. A., and Gaffney, E. A. (2017). Mechanical Cell–Cell Communication in Fibrous Networks: The Importance of Network Geometry. *Bull. Math. Biol.*, 79(3):498–524.

Jansen, K. A., Donato, D. M., Balcioglu, H. E., Schmidt, T., Danen, E. H. J., and Koenderink, G. H. (2015). A guide to mechanobiology: Where biology and physics meet. *Biochim. Biophys. Acta - Mol. Cell Res.*, 1853(11):3043–3052.

Jansen, K. A., Licup, A. J., Sharma, A., Rens, R., MacKintosh, F. C., and Koenderink, G. H. (2018). The Role of Network Architecture in Collagen Mechanics. *Biophys. J.*, 114(11):2665–2678.

Jones, C. A. R., Cibula, M., Feng, J., Krnacik, E. A., McIntyre, D. H., Levine, H., and Sun, B. (2015). Micromechanics of cellularized biopolymer networks. *Proc. Natl. Acad. Sci.*, 112(37):E5117—-E5122.

Jones, C. A. R., Liang, L., Lin, D., Jiao, Y., and Sun, B. (2014). The spatial-temporal characteristics of type I collagen-based extracellular matrix. *Soft Matter*, 10(44):8855–8863.

Joshi, J., Mahajan, G., and Kothapalli, C. R. (2018). Three-dimensional collagenous niche and azacytidine selectively promote time-dependent cardiomyogenesis from human bone marrow-derived MSC spheroids. *Biotechnol. Bioeng.*, 115(8):2013–2026.

Karamichos, D., Brown, R. A., and Mudera, V. (2007). Collagen stiffness regulates cellular contraction and matrix remodeling gene expression. *J. Biomed. Mater. Res. Part A*, 83A(3):887–894.

Kim, D. H. and Wirtz, D. (2013). Focal adhesion size uniquely predicts cell migration. *FASEB J.*, 27(4):1351–1361.

Kim, J., Mao, X., Jones, C. A. R., Feng, J., Sun, B., Sander, L. M., and Levine, H. (2017). Stress-induced plasticity of dynamic collagen networks. *Nat. Commun.*, 8(1).

Kim, J., Zheng, Y., Alobaidi, A. A., Nan, H., Tian, J., Jiao, Y., and Sun, B. (2020). Geometric Dependence of 3D Collective Cancer Invasion. *Biophys. J.*, 118(5):1177–1182.

Kirkpatrick, S., Gelatt, C. D., and Vecchi, M. P. (1983). Optimization by simulated annealing. *Science (80-.).*, 220(4598):671–680.

Kong, F., García, A. J., Mould, A. P., Humphries, M. J., and Zhu, C. (2009). Demonstration of catch bonds between an integrin and its ligand. *J. Cell Biol.*, 185(7):1275–1284.

Lang, N. R., Münster, S., Metzner, C., Krauss, P., Schürmann, S., Lange, J., Aifantis, K. E., Friedrich, O., Fabry, B., Lange, J., Friedrich, O., Münster, S., Lang, N. R., Schürmann, S., Krauss, P., Fabry, B., Metzner, C., Münster, S., Metzner, C., Krauss, P., Schürmann, S., Lange, J., Aifantis, K. E., Friedrich, O., and Fabry, B. (2013). Estimating the 3D pore size distribution of biopolymer networks from directionally biased data. *Biophys. J.*, 105(9):1967–1975.

Lee, B., Zhou, X., Riching, K., Eliceiri, K. W., Keely, P. J., Guelcher, S. A., Weaver, A. M., and Jiang, Y. (2014). A three-dimensional computational model of collagen network mechanics. *PLoS One*, 9(11):1–12.

Lerche, M., Elosegui-Artola, A., Guzmán, C., Georgiadou, M., Kechagia, J. Z., Gulberg, D., Roca-Cusachs, P., Peuhu, E., and Ivaska, J. (2019). Integrin binding dynamics modulate ligand-specific mechanosensing in mammary gland fibroblasts. *bioRxiv*, pages 1–27.

Liang, L., Jones, C., Chen, S., Sun, B., and Jiao, Y. (2016). Heterogeneous force network in 3D cellularized collagen networks. *Phys. Biol.*, 13(6):1–11.

Lindström, S. B., Vader, D. A., Kulachenko, A., and Weitz, D. A. (2010). Biopolymer network geometries: Characterization, regeneration, and elastic properties. *Phys. Rev. E - Stat. Nonlinear, Soft Matter Phys.*, 82(5):2–6.

López-García, M., Selhuber-Unkel, C., Spatz, J. P., Erdmann, T., Schwarz, U. S., and Kessler, H. (2010). Cell Adhesion Strength Is Controlled by Intermolecular Spacing of Adhesion Receptors. *Biophys. J.*, 98(4):543–551.

Lu, P., Takai, K., Weaver, V. M., and Werb, Z. (2011). Extracellular Matrix degradation and remodeling in development and disease. *Cold Spring Harb. Perspect. Biol.*, 3(12):1–24.

Ma, X., Schickel, M. E., Stevenson, M. D., Sarang-Sieminski, A. L., Gooch, K. J., Ghadiali, S. N., and Hart, R. T. (2013). Fibers in the extracellular matrix enable long-range stress transmission between cells. *Biophys. J.*, 104(7):1410–1418.

Malandrino, A., Trepat, X., Kamm, R. D., and Mak, M. (2019). Dynamic filopodial forces induce accumulation, damage, and plastic remodeling of 3D extracellular matrices. *PLoS Comput. Biol.*, 15(4):1–26.

Mammoto, A., Mammoto, T., and Ingber, D. E. (2012). Mechanosensitive mechanisms in transcriptional regulation. *J. Cell Sci.*, 125(13):3061–3073.

Mann, A., Sopher, R. S., Goren, S., Shelah, O., Tchaicheeyan, O., and Lesman, A. (2019). Force chains in cell-cell mechanical communication. *J. R. Soc. Interface*, 16(159):20190348.

Marenzana, M., Wilson-Jones, N., Mudera, V., and Brown, R. A. (2006). The origins and regulation of tissue tension: Identification of collagen tension-fixation process in vitro. *Exp. Cell Res.*, 312(4):423–433.

Mason, D. E., Collins, J. M., Dawahare, J. H., Nguyen, T. D., Lin, Y., Voytik-Harbin, S. L., Zorlutuna, P., Yoder, M. C., and Boerckel, J. D. (2019). YAP and TAZ limit cytoskeletal and focal adhesion maturation to enable persistent cell motility. *J. Cell Biol.*,

218(4):1369–1389.

Mauri, A., Hopf, R., Ehret, A. E., Picu, C. R., and Mazza, E. (2016). A discrete network model to represent the deformation behavior of human amnion. *J. Mech. Behav. Biomed. Mater.*, 58:45–56.

Mickel, W., Münster, S., Jawerth, L. M., Vader, D. A., Weitz, D. A., Sheppard, A. P., Mecke, K., Fabry, B., and Schröder-Turk, G. E. (2008). Robust pore size analysis of filamentous networks from three-dimensional confocal microscopy. *Biophys. J.*, 95(12):6072–6080.

Miroshnikova, Y. A., Jorgens, D. M., Spirio, L., Auer, M., Sarang-Sieminski, A. L., and Weaver, V. M. (2011). Engineering strategies to recapitulate epithelial morphogenesis within synthetic three-dimensional extracellular matrix with tunable mechanical properties. *Phys. Biol.*, 8(2).

Mogilner, A. and Oster, G. (2003). Force Generation by Actin Polymerization II : The Elastic Ratchet and Tethered Filaments. *Biophys. J.*, 84(3):1591–1605.

Moore, S. W., Roca-Cusachs, P., and Sheetz, M. P. (2010). Stretchy proteins on stretchy substrates: The important elements of integrin-mediated rigidity sensing. *Dev. Cell*, 19(2):194–206.

Motte, S. and Kaufman, L. J. (2013). Strain stiffening in collagen i networks. *Biopolymers*, 99(1):35–46.

Müller, K. W., Bruinsma, R. F., Lieleg, O., Bausch, A. R., Wall, W. A., and Levine, A. J. (2014). Rheology of semiflexible bundle networks with transient linkers. *Phys. Rev. Lett.*, 112(23):1–5.

Müller, K. W., Cyron, C. J., and Wall, W. A. (2015). Computational analysis of morphologies and phase transitions of cross-linked, semi-flexible polymer networks. *Proc. R. Soc. A Math. Phys. Eng. Sci.*, 471(2182).

Murtada, S. C., Arner, A., and Holzapfel, G. A. (2012). Experiments and mechanochemical modeling of smooth muscle contraction : Significance of filament overlap. *J. Theor. Biol.*, 297:176–186.

Murtada, S.-I., Kroon, M., and Holzapfel, G. A. (2010). A calcium-driven mechanochemical model for prediction of force generation in smooth muscle. *Biomech. Model. Mechanobiol.*, 9:749–762.

Nam, S., Hu, K. H., Butte, M. J., and Chaudhuri, O. (2016). Strain-enhanced stress relaxation impacts nonlinear elasticity in collagen gels. *Proc. Natl. Acad. Sci.*, 113(20):5492–5497.

Nan, H., Jiao, Y., Liu, R., Chen, G., Liu, L., and Liang, L. (2018). Realizations of highly heterogeneous collagen networks via stochastic reconstruction for micromechanical analysis of tumor cell invasion. *Phys. Rev. E*, 97(3):33311.

Nguyen, D. T., Nagarajan, N., and Zorlutuna, P. (2018). Effect of Substrate Stiffness on Mechanical Coupling and Force Propagation at the Infarct Boundary. *Biophys. J.*, 115(10):1966–1980.

Notbohm, J., Lesman, A., Tirrell, D. A., and Ravichandran, G. (2015). Quantifying cell-induced matrix deformation in three dimensions based on imaging matrix fibers. *Integr. Biol. (United Kingdom)*, 7(10):1186–1195.

Reissner, E. (1981). On finite deformations of space-curved beams. *ZAMP Zeitschrift für Angew. Math. und Phys.*, 32(6):734–744.

Ringer, P., Weißl, A., Cost, A.-l., Freikamp, A., Sabass, B., Mehlich, A., Tramier, M., Rief, M., and Grashoff, C. (2017). Multiplexing molecular tension sensors reveals piconewton force gradient across talin-1. *Nat. Methods*, 14(11).

Ronceray, P., Broedersz, C. P., and Lenz, M. (2016). Fiber networks amplify active stress. *PNAS*, 113(11):2827–2832.

Ross, T. D., Coon, B. G., Yun, S., Baeyens, N., Tanaka, K., Ouyang, M., and Schwartz, M. A. (2013). Integrins in mechanotransduction. *Curr. Opin. Cell Biol.*, 25(5):613–618.

Rycroft, C. H. (2009). VORO++: A three-dimensional Voronoi cell library in C++. *Chaos*, 19(4):1–16.

Schwartz, M. A. (1995). Integrins: Emerging Paradigms of Signal Transduction. *Annu. Rev. Cell Dev. Biol.*, 11(1):549–599.

Seo, B. R., Chen, X., Ling, L., Song, Y. H., Shimpi, A. A., Choi, S., Gonzalez, J., Sapudom, J., Wang, K., Eguiluz, R. C. A., Gourdon, D., Shenoy, V. B., and Fischbach, C. (2020). Collagen microarchitecture mechanically controls myofibroblast differentiation. *Proc. Natl. Acad. Sci. U. S. A.*, 117(21).

Sethi, K. K., Yannas, I. V., Mudera, V., Eastwood, M., McFarland, C., and Brown, R. A. (2002). Evidence for sequential utilization of fibronectin, vitronectin, and collagen during fibroblast-mediated collagen contraction. *Wound Repair Regen.*, 10(6):397–408.

Shi, Q., Ghosh, R. P., Engelke, H., Rycroft, C. H., Cassereau, L., Sethian, J. A., Weaver, V. M., and Liphardt, J. T. (2013). Rapid disorganization of mechanically interacting systems of mammary acini. *Proc. Natl. Acad. Sci.*, 111(2):658–663.

Simo, J. C. (1985). A finite strain beam formulation. The three-dimensional dynamic problem. Part I. *Comput. Methods Appl. Mech. Eng.*, 49(1):55–70.

Simo, J. C. and Vu-Quoc, L. (1986). A three-dimensional finite-strain rod model. part II: Computational aspects. *Comput. Methods Appl. Mech. Eng.*, 58(1):79–116.

Simon, D. D., Horgan, C. O., and Humphrey, J. D. (2012). Mechanical restrictions on biological responses by adherent cells within collagen gels. *J. Mech. Behav. Biomed. Mater.*, 14:216–226.

Simon, D. D., Niklason, L. E., and Humphrey, J. D. (2014). Tissue Transglutaminase, Not Lysyl Oxidase, Dominates Early Calcium-Dependent Remodeling of Fibroblast-Populated Collagen Lattices. *Cells Tissues Organs*, 200(2):104–117.

Stehbens, S. J. and Wittmann, T. (2014). Analysis of focal adhesion turnover: a quantitative live-cell imaging example. *Methods Cell Biol.*, 123:335–346.

Stein, A. M., Vader, D. A., Jawerth, L. M., Weitz, D. A., and Sander, L. M. (2008). An algorithm for extracting the network geometry of three-dimensional collagen gels. *J. Microsc.*, 232(3):463–475.

Stein, A. M., Vader, D. A., Weitz, D. A., and Sander, L. M. (2010). The Micromechanics of Three-Dimensional Collagen-I Gels. *Complexity*, 16(4).

Sukharev, S. and Sachs, F. (2012). Molecular force transduction by ion channels – diversity and unifying principles. *J. Cell Sci.*, 125(13):3075–3083.

Truong, T., Shams, H., and Mofrad, M. R. K. (2015). Mechanisms of integrin and filamin binding and their interplay with talin during early focal adhesion formation. *Integr. Biol. (United Kingdom)*, 7(10):1285–1296.

Van Der Rijt, J. A. J., Van Der Werf, K. O., Bennink, M. L., Dijkstra, P. J., and Feijen, J. (2006). Micromechanical testing of individual collagen fibrils. *Macromol. Biosci.*, 6(9):699–702.

Wang, H., Abhilash, A. S., Chen, C. S., Wells, R. G., and Shenoy, V. B. (2014). Long-Range Force Transmission in Fibrous Matrices Enabled by Tension-Driven Alignment of Fibers. *Biophys. J.*, 107(11):2592–2603.

Wang, Y., Wang, G., Luo, X., Qiu, J., and Tang, C. (2012). Substrate stiffness regulates the proliferation, migration, and differentiation of epidermal cells. *Burns*, 38(3):414–420.

Weng, S., Shao, Y., Chen, W., and Fu, J. (2016). Mechanosensitive subcellular rheostasis drives emergent single-cell mechanical homeostasis. *Nat. Mater.*, 15(9):961–967.

Wiseman, P. W. (2004). Spatial mapping of integrin interactions and dynamics during cell migration by Image Correlation Microscopy. *J. Cell Sci.*, 117(23):5521–5534.

Xie, J., Bao, M., Bruekers, S. M. C., and Huck, W. T. S. (2017). Collagen Gels with Different Fibrillar Microarchitectures Elicit Different Cellular Responses. *ACS Appl. Mater. Interfaces*, 9(23):19630–19637.

Yao, M., Goult, B. T., Chen, H., Cong, P., Sheetz, M. P., and Yan, J. (2014). Mechanical activation of vinculin binding to talin locks talin in an unfolded conformation. *Sci. Rep.*

Yao, M., Goult, B. T., Klapholz, B., Hu, X., Toseland, C. P., Guo, Y., Cong, P., Sheetz, M. P., and Yan, J. (2016). The mechanical response of talin. *Nat. Commun.*, 7(May).

Yeong, C. L. Y. and Torquato, S. (1998). Reconstructing Random Media I and II. *Phys. Rev. E*, 58(1):224–233.

Zemel, A. (2015). Active mechanical coupling between the nucleus, cytoskeleton and the extracellular matrix, and the implications for perinuclear actomyosin organization. *Soft Matter*, 11(12):2353–2363.

Zheng, Y., Nan, H., Liu, Y., Fan, Q., Wang, X., Liu, R., Liu, L., Ye, F., Sun, B., and Jiao, Y. (2019). Modeling cell migration regulated by cell extracellular-matrix micromechanical coupling. *Phys. Rev. E*, 100(4):43303.

Zhou, D., Zhang, L., and Mao, X. (2018). Topological Edge Floppy Modes in Disordered Fiber Networks. *Phys. Rev. Lett.*, 120(6):68003.

Zhu, C., Pérez-González, C., Trepat, X., Chen, Y., Castro, N., Oria, R., Roca-Cusachs, P., Elosegui-Artola, A., and Kosmalska, A. (2016). Mechanical regulation of a molecular clutch defines force transmission and transduction in response to matrix rigidity. *Nat. Cell Biol.*, 18(5):540–548.

Zhu, Y. K., Umino, T., Liu, X. D., Wang, H. J., Romberger, D. J., Spurzem, J. R., and Rennard, S. I. (2001). Contraction of Fibroblast-Containing Collagen Gels: Initial Collagen Concentration Regulates the Degree of Contraction and Cell Survival. *Vitr. Cell. Dev. Biol. - Anim.*, 37(1):10.

Ziegler, W., Gingras, A., Critchley, D., and Emsley, J. (2008). Integrin connections to the cytoskeleton through talin and vinculin. *Biochem. Soc. Trans.*, 36(2):235–239.